

# The axial behaviour of piles driven in chalk

RICHARD J. JARDINE\*, RÓISÍN M. BUCKLEY†, TINGFA LIU‡, THOMAS ANDOLFSSON§, BYRON W. BYRNE||, STAVROULA KONTONE¶, ROSS A. MCADAM\*\*, FABIAN SCHRANZ†† and KEN VINCK‡‡

This paper describes research into the poorly understood axial behaviour of piles driven in chalk. Comprehensive dynamic and monotonic axial testing on 27, mostly instrumented, piles undertaken for the ALPACA joint industry projects is reported and interpreted covering: diameters between 139 mm and 1.8 m; lengths from 3 to 18 m; different pile material types; tip and groundwater conditions; and ages after driving. The experiments show the factors that influence resistance most strongly are: (a) pile end conditions; (b) slenderness ratio and flexibility; (c) shaft material; (d) age after driving; (e) relative water table depth; and (f) whether loading is compressive or tensile. Varying the factors systematically identified a remarkable average long-term shaft resistance range from below 11 kPa to more than 200 kPa for piles driven at the same low- to medium-density chalk test site in Kent (UK). Dynamic and static analyses demonstrate that soil resistances to driving were generally well predicted by the Chalk ICP-18 short-term formulation. Considering the piles' long-term behaviour, the Chalk ICP-18 approach over-predicted capacity, while the widely used CIRIA approach proved over-conservative for most cases. The research enabled the development of a revised 'ALPACA-SNW' long-term capacity assessment method that matches the test outcomes far more faithfully.

**KEYWORDS:** axial capacity; chalk; driven pile; fibre Bragg grating (FBG) sensors; field tests; time dependence

## INTRODUCTION

Jardine *et al.* (2018, 2019) review the considerable uncertainty that exists regarding the behaviour of piles driven in chalk and describe the design of the ALPACA (axial–lateral pile analysis for chalk applying multi-scale field and laboratory testing) and ALPACA-Plus joint industry projects (JIPs) to address short-falls in current knowledge. This paper describes how the two JIPs identified the key factors that control the dynamic and

monotonic, short- and long-term, axial behaviour of a wide range of driven piles. The paper also sets out an improved design approach. Buckley *et al.* (2023) report on the ALPACA studies into cyclic axial loading behaviour, while the 2022 final report of the ALPACA Academic Working Group (AWG), 'Monotonic and cyclic lateral loading of piles in low to medium density chalk', prepared for the JIP sponsors describes the JIPs' parallel investigations into monotonic and cyclic lateral loading.

## BACKGROUND

Chalk occurs worldwide as a very weak to weak biomicrite limestone, composed of lightly cemented silt-sized calcium carbonate ( $\text{CaCO}_3$ ) particles (Mortimore, 2013); it is encountered frequently at foundation depth in northwestern Europe. Conventional design rules have proved critically unable to predict adequately the behaviour of piles driven to support North and Baltic Sea offshore wind turbines (Barbosa *et al.*, 2017; Carotenuto *et al.*, 2018; Buckley *et al.*, 2020a). Refusals have occurred in high-density chalks, while piles have 'run' under self-weight to depths far greater than expected at low- to medium-density sites. Local de-structuration generates thin 'putty' chalk annuli around open-ended piles with undrained shear strength  $S_u < 10$  kPa during driving (Hobbs & Atkinson, 1993; Buckley *et al.*, 2018a; Vinck, 2021), which correlates with natural liquidity indices that are high. Doughty *et al.* (2018) and Vinck (2021) show that dynamic compaction of low- to medium-density chalk at natural water contents leads to similarly weak putties. Axial capacity growth, or set-up, develops after driving and Lord *et al.* (2002) recommend 120 kPa ultimate shaft shear resistances in high-density chalk and 20 kPa for other grades, reducing to 10 kPa for piles with slender shafts that experience marked transient elastic lateral displacements, or 'whip', under driving. Loading tests reported by Barbosa *et al.* (2017) and Vinck (2021) proved capacities that were far higher than predicted, emphasising the need for more economical and reliable design methods.

Buckley *et al.* (2018b) and Buckley *et al.* (2020a) demonstrated that piles driven in chalk share several of the

Manuscript received 1 February 2022; revised manuscript accepted 10 February 2023. First published online ahead of print 13 March 2023.

Discussion on this paper closes on 1 September 2024, for further details see p. ii.

Published with permission by Emerald Publishing Limited under the CC-BY 4.0 license. (<http://creativecommons.org/licenses/by/4.0/>)

\* Department of Civil and Environmental Engineering, Imperial College London, London, UK (Orcid:0000-0001-7147-5909).

† School of Engineering, University of Glasgow, Glasgow, UK (Orcid:0000-0001-5152-7759).

‡ Department of Civil Engineering, University of Bristol, Bristol, UK; formerly Department of Civil and Environmental Engineering, Imperial College London, London, UK (Orcid:0000-0002-5719-8420).

§ Formerly Department of Engineering Science, University of Oxford, Oxford, UK; now SKB AB, Swedish Nuclear Fuel and Waste Management Co., Solna, Sweden (Orcid:0000-0002-5719-8420).

|| Department of Engineering Science, University of Oxford, Oxford, UK (Orcid:0000-0002-9704-0767).

¶ Department of Civil Engineering, University of Patras, Patras, Greece; Visiting Reader at Imperial College London, London, UK (Orcid:0000-0002-8354-8762).

\*\* Formerly University of Oxford, Oxford, UK; now Orsted Power (UK) Ltd, London, UK (Orcid:0000-0003-0292-3549).

†† Formerly Department of Engineering Science, University of Oxford, Oxford, UK; now Office of the Tyrolean Regional Government, Innsbruck, Austria (Orcid:0000-0001-8871-091X).

‡‡ Department of Civil and Environmental Engineering, Imperial College London, London, UK (Orcid:0000-0002-0990-0895).

fundamental features captured in the ICP-05 (Jardine *et al.*, 2005) design approaches for sands and clays, as follows.

- Base resistances  $q_b$  and local shaft radial effective stresses  $\sigma'_{rf}$  and shear resistances  $\tau_{rz}$  correlate linearly with local cone penetration test (CPT) tip resistance  $q_t$ .
- Local  $\sigma'_{rf}$  and  $\tau_{rz}$  reduce sharply as relative pile tip depth  $h$  (normalised by  $R^* = (R_{outer}^2 - R_{inner}^2)^{0.5}$ ) grows during driving.
- Axial capacities vary markedly with time after installation, with long-term shaft resistances remaining affected by  $h/R^*$  and local failure being governed by a Coulomb law with  $\tau_{rzf} = \sigma'_{rf} \times \tan(\delta')$ .
- Laboratory interface ring-shear tests provide accurate operational  $\delta'$  angles  $\approx 31$ – $32^\circ$ .

Buckley (2018) concluded that  $\sigma'_{rf}$  also varies with pile diameter-to-wall-thickness ratio  $D/t_w$  during driving. Working with a sparse set of un-instrumented tension and dynamic tests on open tubular steel piles driven at St Nicholas at Wade (SNW) in the UK and the Wikinger Baltic Sea windfarm, Jardine *et al.* (2018) and Buckley *et al.* (2020a) proposed Chalk 'ICP-18' approaches for soil resistance to driving (SRD) and long-term capacity. A tension-to-compression shaft capacity ratio of unity was assumed, as found with clays, although a ratio  $\approx 0.75$  applies in sands due to principal stress axis rotation effects (Jardine *et al.*, 2005) and 'Poisson' straining of pile shafts (De Nicola & Randolph, 1993). However, analysis of other tests on large tubular steel piles driven at French and German chalk sites by Vinck (2021) and Vinck *et al.* (2023) indicated a lower ratio  $\approx 0.5$ , including cases where the pile's internal plug had been removed by coring.

Implicit in Chalk ICP-18 is marked post-installation set-up. Buckley (2018) interpreted ageing trends from multiple monotonic tension tests on small piles driven (above the water table) at SNW and compressive beginning-of-restriking (BoR) capacities established from dynamically instrumented large piles driven offshore at the Wikinger Baltic windfarm site. Buckley (2018) normalised these capacities by compressive end-of-driving (EoD) SRDs obtained by signal matching of instrumented dynamic records. Ciavaglia *et al.* (2017) noted similar trends from tension tests on other piles driven (above the water table) at SNW. The interpretation by Buckley *et al.* (2018a) of the onshore SNW tension tests' slow initial capacity growth, followed by marked gains over the subsequent months, did not recognise that the tension shaft capacities could be considerably lower than those available at the same age in compression. The like-for-like offshore EoD and BoR trends from Wikinger indicated final set-up ratios that reduced with  $h/R^*$  and progressed more rapidly offshore than at SNW (see Buckley *et al.* (2020a)).

## RESEARCH AIMS

The ALPACA and ALPACA-Plus JIPs aimed to develop reliable, fundamentally based, practical design approaches. As set out by Jardine *et al.* (2019), multi-scale field experiments were conducted on 41 piles driven at SNW, as shown in Fig. 1(a), with their heights, diameters and relative position to the water table shown in Fig. 1(b). In addition to the cyclic and lateral loading studies, comprehensive programmes of dynamic and monotonic axial experiments were undertaken on 27 piles. Most were equipped with diametrically opposed strings of fibre Bragg grating (FBG) fibre-optical axial strain gauges, configured and processed as recommended by Doherty *et al.* (2015) and Burd *et al.* (2020). The influences of groundwater conditions, pile

material, embedded length ( $L_p$ ), diameter ( $D$ ) and wall thickness ( $t_w$ ) on SRD, set-up, loading sense (i.e. tension or compression) and long-term axial load–displacement behaviour were examined systematically over 4 years.

## ST NICHOLAS AT WADE SITE

The test site comprises a former quarry, located  $\approx 2$  km inland and 15 km west of Margate, Kent at UK grid TR 25419 66879. Buckley *et al.* (2018a) and Vinck *et al.* (2022) describe the Margate and Seaford white chalks encountered and provide full details of the chalk's geotechnical profiles and properties as measured through intensive in situ and laboratory testing. They also note that tectonism, periglacial activity, weathering and geomorphology control the chalk's structure. Most weathered material has been removed, leaving CIRIA grade B2 (Lord *et al.*, 2002) structured, very weak to weak, low- to medium-density white structured chalk with closed to slightly open stained joints and beds of 250 mm average thickness, along with mainly vertically oriented micro-fissures spaced at 10 to 25 mm apart.

The water table lies at  $\approx 5.5$  to 6 m depth,  $\approx 0.9$  m above ordnance datum (AOD); suctions measured at 3 m depth with in situ tensiometers fluctuated around 30 kPa. Vinck *et al.* (2022) report on the piezocone (CPTu) and seismic CPT (SCPT) soundings undertaken close to each pile, nine of which are shown in conjunction with the pile tests reported later in this paper. Vinck *et al.* (2022) also report on cone pressuremeter testing, P–S logging, cross-hole and down-hole seismic testing, and provide profiles of index, oedometer, simple shear, unconfined compression and Brazilian tension tests. Multiple locally instrumented (drained and undrained) triaxial tests were conducted on block samples and cores from Geobore-S wireline rotary boreholes. Analysis of the data by Vinck *et al.* (2022) included detailed assessments of sample size effects and small-strain stiffness anisotropy. Liu *et al.* (2023) report further on the chalk's behaviour under effective stresses up to 13 MPa, as developed beneath the pile tips during driving.

An additional highly relevant topic is how effective normal stress level, interface material, ageing, corrosion and testing procedure affect the interface shearing resistance and shaft radial stress conditions developed around steel piles driven in chalk. Laboratory research by Vinck (2021) found that corrosion affects ultimate  $\delta'_{ult}$  mildly, giving angles that exceed destructured chalk's critical state  $\phi'_{cs} \approx 31^\circ$  for all cases except (in the short term) stainless steel. However, corrosion is shown later to affect axial capacity markedly through, it is argued, radial effective stress growth around corroding steel piles, in a process comparable to that noted around steel bars in corroding reinforced concrete (Su & Zhang, 2015). The reactions draw in additional air, water and salt molecules to generate products of lower density that expand out, while being constrained radially by very stiff chalk. Noting that air can flow through any open fissures available above the water table, and the need to capture offshore conditions, Vinck (2021) examined how air and salinity affect surface corrosion mass loss rates of prismatic samples (termed coupons) cut from a typically rough pile shaft in contact with chalk. The reaction rates developed over periods of up to 67 days, expressed in  $\mu\text{m}$  steel loss per year, were

- ten times slower in isolated tests than when exposed to air
- three or more times faster with saline than fresh groundwater
- comparable between various oxidisable construction steels
- ninety times slower with stainless steel and absent with concrete.

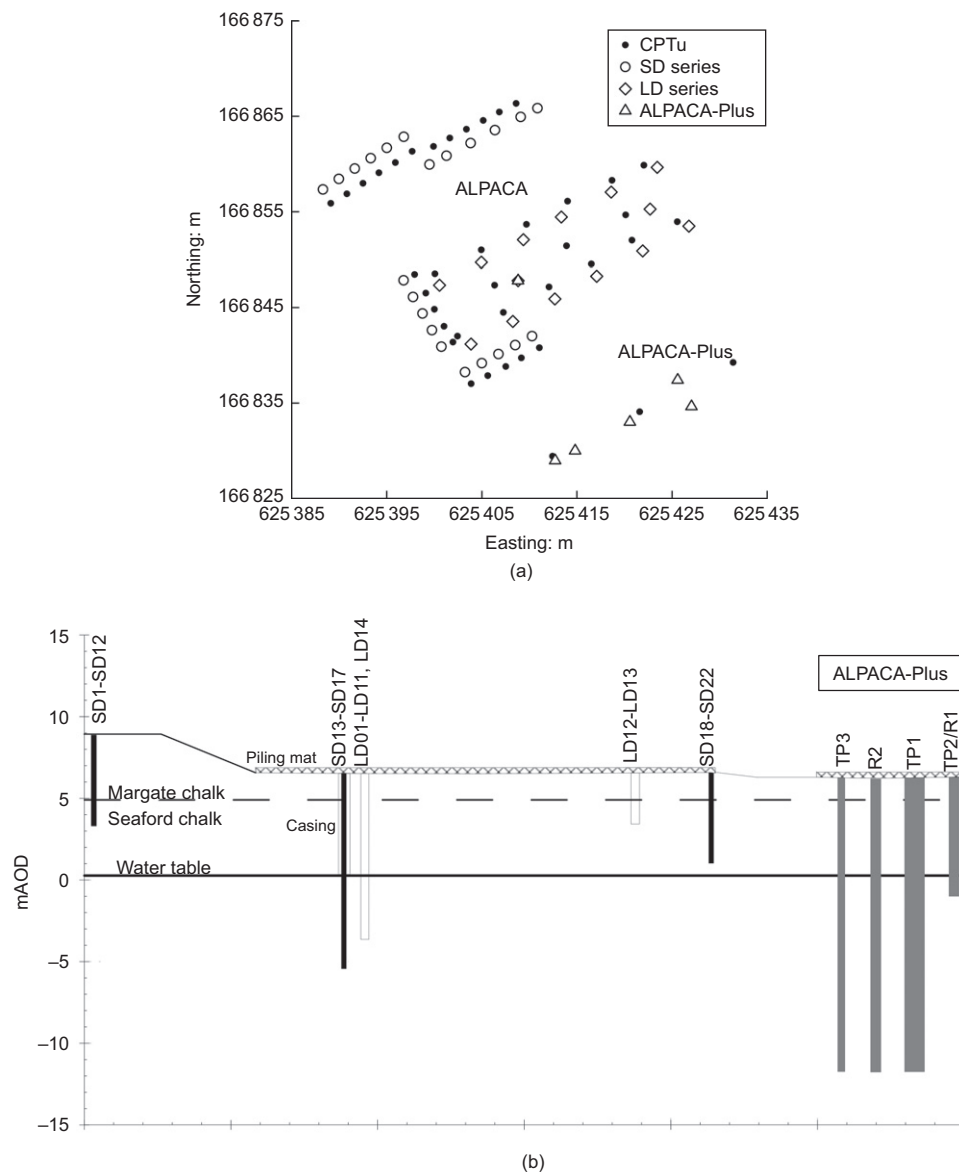


Fig. 1. Pile testing layout at SNW: (a) plan; (b) section showing locations, diameters and levels relative to the water table for ALPACA LD, SD and ALPACA-Plus piles

Table 1. Summary for ALPACA LD open steel piles

Code	Steel grade	$D$ : m	$t_w$ : mm	$L_p$ : m	$H_{plug}$ : m*	EoD $\tau_{avg}$ : kPa	EoD $q_{ba}/q_t$	Age†: days	Test $\tau_{avg}$ : kPa	Comment‡
LD5	X80	0.508	20.6	10.16	0.96	21.1	0.47	219	36.7	Compression
LD6	X80	0.508	20.6	10.16	0.88	28.0	0.52	211	39.1	
LD7	X80	0.508	20.6	10.16	1.02	20.4	0.58	260	59.7 (70.4)§	
LD12	X80	0.508	20.6	3.05	1.07	31.3	0.40	221	112.0	
LD13	X80	0.508	20.6	3.05	0.99	19.8	0.42	294	89.2	
LD14	X80	0.508	20.6	10.16	0.90	24.8	—	66	21.2	

\*Chalk plug height above the original ground level.

†Age: at first monotonic test.

‡Tests in tension unless otherwise noted.

§Average shaft resistance  $\tau_{avg} = 59.7$  kPa determined for top 9.5 m embedded section directly from FBGs;  $\tau_{avg} = 70.4$  kPa derived for full length, estimated from 9.5–10.16 m section of tension tests (LD5 and LD6), assuming compression-to-tension ratio of 2.

||PDA data quality of LD14 assessed as poor following Buckley's (2018) approach, so tabulated value represents the average EoD  $\tau_{avg}$  for all LD piles.

Other laboratory testing by Doughty *et al.* (2018) showed that the stiffness and shearing resistances of chalk that is destructured to putty increase over time through both consolidation and carbonate re-bonding.

#### TEST PILES

Tables 1–4 summarise the considered test piles' sizes, tip conditions and materials. The FBG strain gauges, with the 0.15 to 0.6 m spacings detailed in Table 5, were installed and monitored following the protocols set out by Doherty

*et al.* (2015) and gave high-resolution measurements over the piles' 3.05 to 18 m embedded lengths. Applying temperature corrections and Savitzky–Golay filtering to reduce scatter led to well-defined average axial force profiles from which local shaft resistances were generated. The latter accounted for pile plus chalk plug weights and upthrust due to any positive base water pressures. All but one of the monotonic tests considered tension loading conditions. All piles that were subsequently extracted showed fully retained internal cores with clean tension fractures at their bases. The average long-term internal skin friction required to lift the internal cores was  $\approx 2$  kPa for the longer large-diameter (LD) piles and  $\approx 8$  kPa for the largest (1.8 m outer diameter (OD)) ALPACA-Plus pile. The distributions of internal shaft friction developed during the single compression test are not known and are implicitly included in the overall base and shaft resistances indicated by the FBG strain gauges. Tests reported by Vinck (2021) on other open instrumented steel piles driven in chalk, including one whose internal chalk core had been removed prior to testing, indicate that internal shaft resistance alone could not explain their higher compressive than tension axial shaft capacities.

Multiple Mitutoyo SJ-210 gauge measurements were made on the ALPACA piles that indicated pre-driving centre-line-average  $R_{CLA}$  pile shaft roughness means of 15.4, 10.1 and 14.2  $\mu\text{m}$  for the oxidisable steel LD, smaller-diameter (SD) and ALPACA-Plus piles, respectively, while the stainless steel and concrete shafts gave 6.0 and 3.8  $\mu\text{m}$ . Noting the chalk's  $\approx 3$   $\mu\text{m}$   $D_{50}$  grain size, all pile shafts provided fully rough interfaces; see Lings & Dietz (2005).

#### Large-diameter ALPACA series

The open-ended, oxidisable X80 steel, FBG instrumented, tubular LD piles had 508 mm outside diameters ( $D$ ) and 20.6 mm wall thicknesses ( $t_w$ ), giving relatively low  $D/t_w \approx 24.7$ . Most were driven in November 2017 to tip depths of 3.05 m ( $\approx 3$  m above the water table with  $L_p/D = 6$ ) or 10.16 m ( $\approx 4.2$  m below the water table with  $L_p/D = 20$ ).

#### Smaller-diameter ALPACA series

The SD series included 12 in number 139 mm dia. steel tubular piles (two with FBG strings) fabricated from various steels, driven to tip depths above the water table. Ten open piles were driven from ground level to  $38 < L_p/D < 40$ ; their 8 to 10 mm wall thicknesses gave  $14 < D/t_w < 17.5$ . Tip conditions were investigated by driving two otherwise identical closed-ended steel SD piles. A 200 mm square pre-cast reinforced concrete pile, with  $D^* = 226$  mm and  $L_p/D^* \approx 24$ , based on equivalent base area, and a pair of 'crenulated' SM-J steel sheet piles were also driven, with  $L_p/D^* \approx 18$  to 19 when  $D^*$  is defined from perimeter length/ $\pi = 290$  mm.

Four further 12 m long, 139 mm OD open steel piles and one additional 200 mm factory pre-cast concrete pile, were driven to 6.15 m through pre-bored cased holes that isolated their shafts from the unsaturated chalk.

#### ALPACA-Plus series

The ALPACA-Plus piles had higher  $D/t_w$  ratios (41 to 72) and 508 mm, 1220 mm and 1800 mm outside diameters. Axial testing in October 2021 concentrated on piles driven to  $L_p = 18$  m, with  $10 \leq L_p/D \leq 35$ . Table 4 details how BoR dynamic data recorded over the first blows applied after operational driving pauses, and at two later dates.

#### ANALYSIS OF DRIVING BEHAVIOUR

The open tubular LD and SD piles required between 9 and 55 blows per quarter metre (bpqm) with the hammers detailed in Table 6 and had total driving times from 2 to 14 min. All open piles generated chalk cores that rose well above ground level, confirming relatively little radial displacement out into the chalk mass. Fig. 2 shows how the volume extruded above ground compared to that of the embedded steel,  $V_{\text{pag}}/V_{\text{steel}}$ , fell systematically with  $L_p/D$ ; open pile cores rarely rise above ground level in sands and clays.

The 200 mm square concrete piles required up to 308 bpqm over up to 81 min to reach target depths with the hammers deployed; the sheet piles required up to 100 bpqm and  $\approx 20$  min of driving. Table 6 summarises estimates for the average non-dimensional velocity  $V = vD^*/c_h$  (with  $v$  = final penetration/driving time) adopting piezocone dissipation test  $c_h = 7 \times 10^{-4}$  m<sup>2</sup>/year (Vinck *et al.*, 2022), and  $D = 2R^*$  for open piles, after Carter *et al.* (1980). Finnie & Randolph (1994) argue that penetration is fully undrained for  $V > 30$  and principally undrained beneath closed-ended piles if  $V$  ranges from 2 to 20. Table 6 indicates low degrees of drainage during driving beneath the larger open piles and higher degrees for the concrete and sheet piles. Dissipation tests at SNW with 43.7 mm dia. piezocones showed pore pressures sensed at the cone shoulders dissipating fully within 80 s. Scaling up by  $(D^*/D_{\text{CPT}})^2$  leads to  $t_{0.5}$  estimates for the pile tip areas ranging from  $\approx 400$  s to  $\approx 2$  h for the smallest to largest diameter piles. As listed in Table 6, substantial dissipation is likely to have occurred over the driving pauses identified in Table 4.

Pile driving analyser (PDA) strain gauges and accelerometers were mounted on all piles and recorded at 40 kHz. Iterative wave-matching analyses, which applied the shaft and base resistance models in IMPACT (Randolph, 2008), indicated how shaft shear stresses evolved locally as pile tips advanced. Buckley *et al.* (2020b) considered both FBG and PDA measurements and described how modelling parameters were selected and shaft resistances taken as applying over only the outside shaft areas. The FBG measurements agreed well with high-frequency conventional PDA measurements, and the EoD datasets provided key information on the piles' initial axial resistance profiles. Buckley *et al.* (2020b), Cathie *et al.* (2022) and Wen *et al.* (2023) showed that rigorously conducted stress wave matches provide the best available proxy means of measuring instantaneous EoD resistances, which cannot be measured statically in cases where set-up progresses rapidly. These authors showed that, if conducted and interpreted carefully, stress wave analyses of instrumented dynamic re-strike tests provide shaft capacity estimates that are compatible with trends inferred from static testing. However, dynamic testing offers the only practical means of monitoring rapid early-age set-up, such as occurs in chalks.

Tables 1–4 summarise the interpreted overall EoD shaft and base resistances, while Figs 3(a)–3(e) illustrate the various series' EoD shaft friction profiles. Piles SD20 (open steel), SD5 (closed steel) and SD19 (concrete) represent the SD cases. The long and short 508 mm piles are typified by LD5 and LD13; traces are also shown for the TP1 and TP3 ALPACA-Plus piles. The open piles' average, compressive,  $\tau_{\text{avg}}^{\text{EoD}}$  values range from 19.8 to 32.2 kPa (including six 'SD' piles from Buckley *et al.* (2018a)) giving means and coefficient of variation (CoV) of 24.8 kPa and 0.14, respectively. Also shown are representative  $q_t$  traces from nearby CPTs and Chalk ICP-18 SRD predictions from equations (1) and (2), which capture the sharp reductions of local shear resistances with increasing  $h/R^*$ .

$$\tau_{\text{rzi}} = \sigma'_{\text{ri}} \tan \delta'_{\text{ult}} \quad (1)$$

**Table 2. Summary for ALPACA SD steel tubular piles**

Code	Steel grade	$D$ : m	$t_w$ : mm	$L_p$ : m	$H_{\text{plug}}$ : m*	EoD $\tau_{\text{avg}}$ : kPa	EoD $q_{ba}/q_t$	Age: days	Test $\tau_{\text{avg}}$ : kPa	Comment†
SD5	Drill casing	0.139	9.7	5.50	—	19.7	0.82	3	73.4	Closed
								276	81.3	Re-test
SD7	Drill casing	0.139	9.4	5.40	—	19.7‡	—	330	142.3	Closed
								332	134.8	Re-test
SD8	Drill casing	0.139	9.6	5.44	0.56	26.0	0.73	2	57.5	Open
								308	55.4	Re-test
SD12	Drill casing	0.139	10.2	5.35	0.65	24.8‡	—	318	69.3	Open
SD13	Stainless	0.139	8.0	5.42	$\approx 0.46$	25.8	0.67	126	10.7	Cased, open
SD14	Drill casing	0.139	9.8	5.31	$\approx 1.30$	22.5	0.59	127	13.1	Cased, open
SD15	S355	0.139	8.6	4.92	$\approx 1.69$	27.4	0.74	128	18.7	Cased, open
SD16	L80/N80	0.139	10.0	5.41	$\approx 1.18$	20.4	0.58	129	17.0	Cased, open
SD18	Stainless	0.139	8.0	5.49	0.26	24.8‡	—	125	30.2	Open
SD20	Drill casing	0.139	10.1	5.50	0.30	23.3	0.68	126	57.0	Open
SD21	S355	0.139	8.2	5.48	0.33	26.3	0.70	127	50.9	Open
SD22	L80/N80	0.139	9.6	5.48	0.0	24.5	0.72	128	51.0	Open

\*Chalk plug height above the original ground level.

†Tests in tension unless otherwise noted.

‡PDA data quality judged as poor following Buckley's (2018) approach. Tabulated values represent: (a) either the average EoD  $\tau_{\text{avg}}$  for all open-ended tubular pile cases, = 24.8 kPa, or (b) EoD  $\tau_{\text{avg}}$  of 'twin' pile(s) with similar geometry.

**Table 3. Summary for ALPACA SD closed-ended sheet and precast concrete piles**

Code	Material	$D_{\text{equ}}$ : m*	$t_w$ : mm	$L_p$ : m	EoD $\tau_{\text{avg}}$ : kPa	EoD $q_b/q_t$	Age: days	Test $\tau_{\text{avg}}$ : kPa	Comment†
SD10	Sheet/S355 steel	0.290	12.2	5.42	37.1	0.99	3	48.0	System limit, not failed
							170	146.2	Re-test, failed
SD9	Sheet/S355 steel	0.290	11.0	5.35	37.1‡	—	317	204.7	System limit, not failed
SD17	Precast concrete	0.255	—	4.93	83.3‡	—	129	134.6	Not failed
							155	98.2	Re-test, failed
SD19	Precast concrete	0.255	—	5.40	83.3	0.89	156	126.1	Failed

\*Equivalent diameter  $D_{\text{equ}} = \text{perimeter}/\pi$ .

†Tests in tension unless otherwise noted.

‡PDA data quality judged as poor following Buckley's (2018) approach. Tabulated values represent: (a) either the average EoD  $\tau_{\text{avg}}$  for all open-ended tubular pile cases, = 24.8 kPa, or (b) EoD  $\tau_{\text{avg}}$  of 'twin' pile(s) with similar geometry.

**Table 4. Summary for ALPACA-Plus open steel series**

Code	Material	$D$ : m	$t_w$ : mm	$L_p$ : m	$H_{\text{plug}}$ : m*	EoD $\tau_{\text{avg}}$ : kPa	EoD $q_{\text{ba}}/q_t$	Age: days	Type†	Test or BoR $\tau_{\text{avg}}$ : kPa	BoR $q_{\text{ba}}/q_t$
TP1	S355	1.8	25	7.94	—	22.8	0.40	0.09	Restrike	79.6	0.50
				18.0 (EoD)	1.41	26.2	0.61	373	AST	57.0	
TP2	S460	1.22	24.6	3.14	—	23.4	0.50	0.05	Restrike	63.0	0.60
				7.3 (EoD)	0.83	22.1	0.50	409	LS		
TP3	S355	0.508	12.5	7.90	—	24.8‡	—	0.05	Restrike	59.3	0.50
				18.0 (EoD)	1.20	26.9	0.50	380	AST	24.9	
R1	S460	1.22	24.6	4.11	—	20.7	0.40	0.06	Restrike	66.0	0.60
				7.3 (EoD)	0.79	31.3	0.50	415	L1W/LS		
R2	S460	1.22	24.6	7.19	—	32.2	0.50	0.64	Restrike	64.1	0.60
									(BoR1)		
				17.97 (EoD)	1.36	24.2	0.61	5.2	Restrike	76.2	0.73
									(BoR2)		
								421	Restrike	117.4	0.82
									(BoR3)		

\*Chalk plug height above the original ground level.

†Test type: AST, axial static tension; BoR, beginning of restriking; LS, lateral static; L1W, lateral one-way cyclic (see the 2022 final report of the ALPACA AWG to the JIP sponsors).

‡PDA data quality judged as poor following Buckley's (2018) approach. Tabulated values represent: (a) either the average EoD  $\tau_{\text{avg}}$  for all open-ended tubular pile cases = 24.8 kPa, or (b) EoD  $\tau_{\text{avg}}$  of 'twin' pile(s) with similar geometry.

**Table 5. Fibre Bragg grating (FBG) sensor configuration**

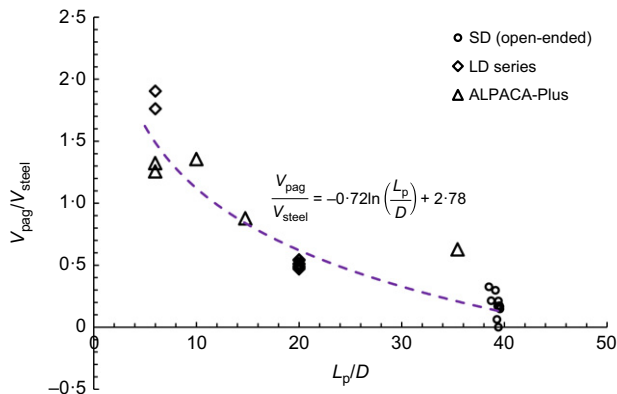
Series	Number*	Top: mbgl	Bottom: mbgl	Spacing	Temperature sensor depth: mbgl
SD12	12	0.12	5.08	$\approx 0.28$ m to 1.23 mbgl, then 0.55 m	—
Short LD	12	0.15	2.85	0.15 m to 0.75 mbgl, then 0.3 m	—
Long LD	12	0.5	9.5	0.5 m to 2.5 mbgl, then 1 m	9.4 (only with LD14)
TP1, TP3	29 (+2)†	0.62	17.85	$\approx 0.61$ m throughout	9.18, 17.8
TP2, R1	17 (+2)†	−0.15	7.15	$\approx 0.33$ m to 2.15 mbgl, then 0.5 m	−0.15, 6.65 (only with TP2)

\*Number of sensors in one FBG string; all piles instrumented with two diametrically opposite strings.

†Value in parentheses is the number of fibre optic temperature sensors.

**Table 6. Ranges of normalised velocity  $V$  and upper-bound full drainage elapsed times after end of driving**

Series	Geometry/end condition	$R^*$ : m	Normalised $V$	Upper-bound $t_{95}$ : min	Hydraulic hammer (ram mass)
SD	Open	0.035	0.52–1.50	3.4	Delmag (1.4 t)
SD	Closed	0.070	0.36–1.20	13.4	Delmag (1.4 t)
SD	Sheet	0.057	0.24	9.0	Delmag (1.4 t)
SD	Concrete	0.113	0.10–0.16	35.5	Delmag (1.4 t)
LD	Open	0.100	0.79–2.09	27.9	Juntann SHK-4 (4 t)
					Juntann HHK-5A (5 t)
ALPACA-Plus (1.8 m OD)	Open	0.211	2.74	123.4	BSP CG240 (16 t)
ALPACA-Plus (1.22 m OD)	Open	0.171	1.64–2.48	81.8	BSP CX110 (9 t)
ALPACA-Plus (0.508 m OD)	Open	0.079	0.50	17.2	BSP CX110 (9 t)

**Fig. 2. Variation of the ratio between the above-ground chalk plug volume ( $V_{\text{pag}}$ ) and embedded steel volume ( $V_{\text{steel}}$ ) against  $L_p/D$** 

$$\sigma'_{\text{ri}} = 0.031 q_t \left( \frac{h}{R^*} \right)^{-0.481 (D/t_w)^{0.145}} \quad (h/R^* \geq 6) \quad (2)$$

Comparison of the total EoD shaft load between the predictions  $Q_s$  integrated from the above expressions, taking  $\delta'_{\text{ult}} = 32^\circ$  and the signal-matching outcomes indicated a mean calculated-to-measured ( $Q/Q_m$ ) ratio of 1.00 (with CoV = 0.38) for the open-ended piles listed in Tables 1–4 with reliable  $\tau_{\text{avg}}^{\text{EoD}}$  values. Open piles with the lowest  $L_p/D$  (=6) values developed the highest EoD resistances, reflecting their lower  $h/R^*$  values and consequently smaller local  $\tau_{\text{rzi}}$  reductions. Closed-ended steel SD5 showed the lowest (reliable)  $\tau_{\text{avg}}^{\text{EoD}}$  value, which fell well below the ICP-18 predictions, reflecting the larger strains and greater destruction that develop beneath closed pile tips. Baligh *et al.*

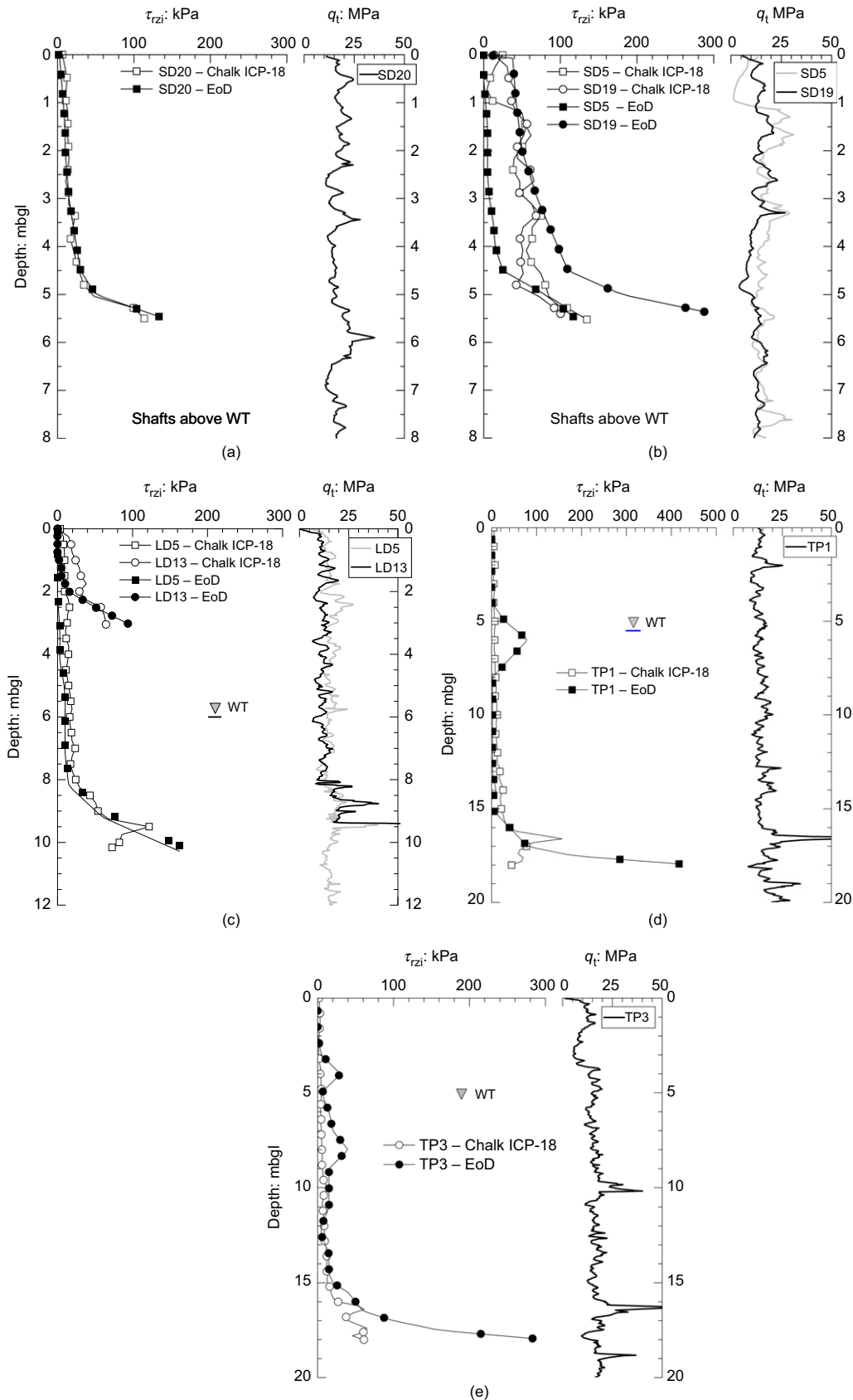


Fig. 3. Profiles of CPT resistance and shaft friction from end-of-driving (EoD) PDA analyses compared against short-term Chalk ICP-18 predictions: (a) SD series – open-ended piles; (b) SD series – closed-ended piles; (c) LD series; (d) ALPACA-Plus TP1; (e) ALPACA-Plus TP3

(1987) showed strains reduce systematically with  $D/t_w$  during undrained penetration and are typically an order of magnitude smaller under open tubular piles than closed-ended piles. The sheet and concrete piles'  $\tau_{avg}^{EoD}$  (37.1 and 83.3 kPa,

respectively) matched ICP-18 estimates more closely, although their slow driving may have permitted more drainage; lower SRDs might have applied under undrained conditions.



Figure 4 presents the signal-matched EoD  $q_b$  values, evaluated over closed piles' full areas and open piles' annuli, normalised by  $q_t$  (averaged within  $1.5D$  of the pile tip) and plotted against  $D/t_w$  (taking 2 for closed piles). The EoD  $q_b/q_t$  ratios decline with  $D/t_w$ , as expected by Baligh *et al.* (1987), up to  $D/t_w$  ratios of at least 25. Equation (3) leads to a better and more conservative fit to the data than the Chalk ICP-18's tentatively suggested  $q_b/q_t \approx 0.6$ .

$$\frac{q_b}{q_t} = (D/t_w)^{-0.175} \quad (3)$$

Pile set-ups were gauged by monotonic and (for ALPACA-Plus) dynamic BoR tests. Noting that the 5.2 day re-strike on R2 may have set back its subsequent ageing, the 421 day BoR provides a lower bound to the long-term resistance of an equivalent 'virgin' pile, although Vinck (2021) noted that the impact of early re-strikes diminish over time. Fig. 5 plots against age the average re-strike set-up factors derived from BoR tests conducted on piles whose capacities were primarily developed below the water table, divided by the EoD value from the last blow before any pause commenced, along with  $t_{95}$  times estimated by scaling up the piezocone dissipation test  $t_{95}$  times by  $(D^*/D_{CPT})^2$  as explained earlier. The normalised depths  $L_p/D$ , to which tips had advanced before each 'test' are also indicated. Table 6 identifies the early-age time ranges over which re-consolidation contributed to set-up. Set-up varies with  $L_p/D$ , as noted in full-scale offshore Winkler pile tests by Buckley *et al.* (2020a). The average set-up trend from eight Winkler piles covering  $0.26 \leq L_p/D \leq 14.9$  with a mean  $\approx 6.8$  is shown plotting close to the  $L_p/D = 10$  SNW trend curve in Fig. 5. Tentative  $L_p/D$  contours are plotted whose interpretation combined: (a) BoR data; (b) trends from the monotonic tension tests described below (accounting for the tension-to-compression shaft capacity ratio); and (c) BoR tests on multiple 0.61 m dia. open steel piles driven in 2021 at Tilbury  $\approx 70$  km east in the (same) Margate and Seaford formations (Wang, 2021).

Further insight into early-age set-up is given in Fig. 6, where pile R2's signal-matched  $\tau_{rzi}$  EoD and three BoR  $\tau_{rz}$  profiles are compared, covering its first re-strike (with  $L_p = 7.2$  m) and two later restrikes performed after finally driving to 18 m.

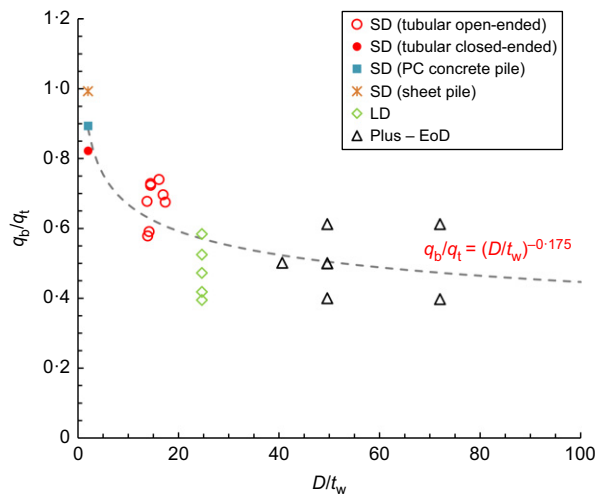


Fig. 4. Normalised bearing pressure ( $q_b/q_t$ ) plotted against piles'  $D/t_w$  at EoD (note:  $q_b$  evaluated over the closed piles' full areas and the open piles' steel annuli;  $D/t_w$  taken as 2 for closed piles)

## MONOTONIC TESTING

The tension tests all reacted against steel, concrete or timber surface pads, except for TP1, which required reaction piles. Reaction piles and kentledge were also employed for the single compression test. Fig. 7 shows the main components of the testing systems deployed. Displacements were recorded by at least three transducers, referenced to distant datum points and placed at equal angles about the pile axis. Potentiometer devices were used for the LD series tests, while linear variable differential transformers (LVDTs) were employed for the SD tests. Awnings reduced the impact of sun and wind variations. Hydraulic jacks applied steady loading between maintained load stages, the durations of which gradually extended to an hour once creeping became significant. Load cell calibrations were checked when

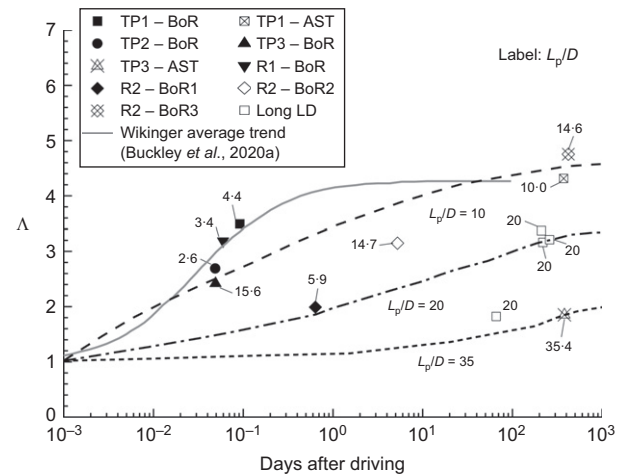


Fig. 5. Variation with time of 'compressive'  $\Lambda$  set-up factors for shaft friction from dynamic restrike and monotonic tension tests on (mainly submerged) ALPACA-Plus and LD piles, showing  $L_p/D$  ratios and tentative contours. Average trend also shown from eight 'Winkler' offshore piles with mean chalk  $L_p/D = 6.8$ , from Buckley *et al.* (2020a)

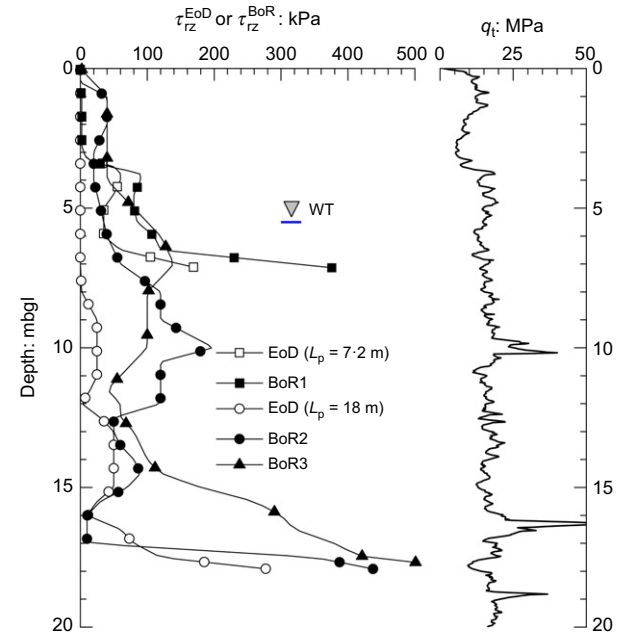


Fig. 6. Short- and longer-term set-up shown by EoD and beginning-of-restriking (BoR) shaft resistance profiles of the ALPACA-Plus pile R2 (see Table 4). CPT profile also shown



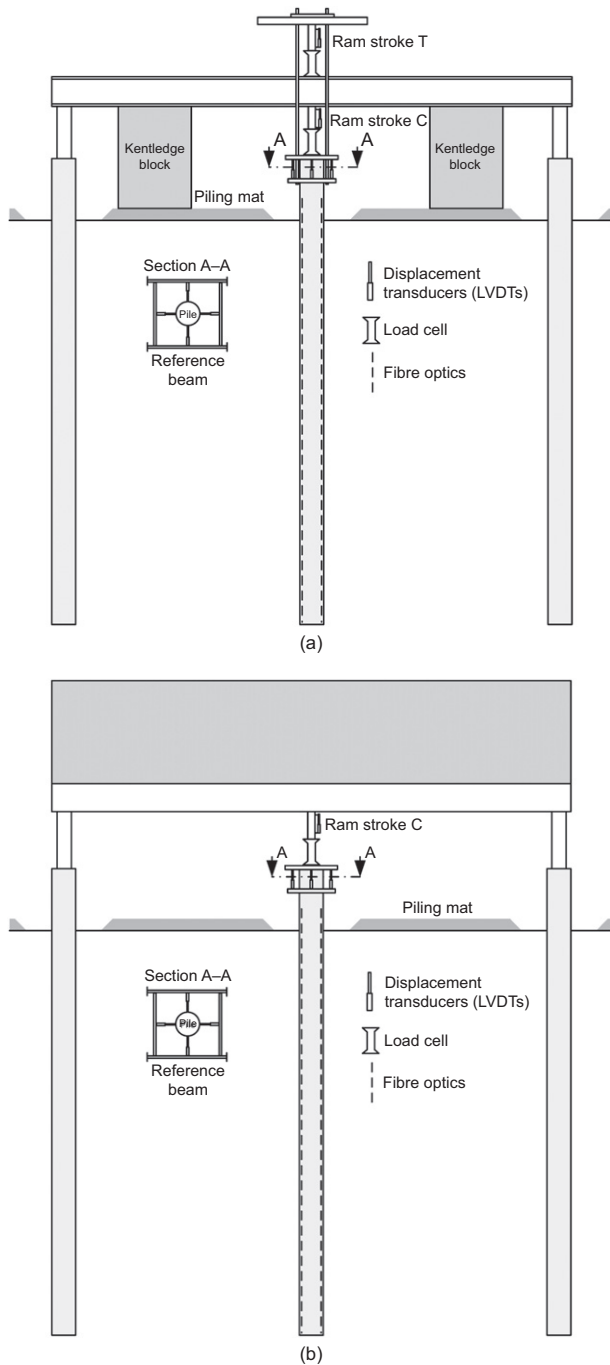


Fig. 7. Schematic arrangements for (a) tension and (b) compression pile tests

required and failure was defined by semi-logarithmic creep movement rates ( $k_s$ ) remaining  $> 2$  mm/log ( $t$ ), 1 h after applying the last load step. Most tests involved eight to ten load stages and ended within a day.

The piles showed apparently near linear load–displacement behaviour up to relatively ( $< 6$  kPa) low threshold  $\tau_{avg}$  values. Analysis of the global initial linear response stages of the ALPACA tests made through the approach of Randolph & Wroth (1978), re-derived for tension, led to the results listed in Table 7. Overall, the global operational shear moduli, covering all zones, found over the limited linear range amounted be around 1/4 of corresponding seismic CPT  $G_{vh}$  values. Matthews *et al.* (2000) noted similarly marked discrepancies applying to shallow foundation loading in chalk, which they ascribed to natural discontinuities.

The piles' average shaft shear stresses  $\tau_{rz}$  values at failure varied widely, from below 11 to over 200 kPa, depending on multiple factors. The analysis below considers separately piles installed entirely (a) above or (b) below the water table and (c) those that spanned both conditions.

#### Above the water table

Load tests are summarised as curves of average  $\tau_{rz}$  against non-dimensional pile head displacement  $w/D$ , or  $w/D^*$  for concrete and sheet piles, whose shear resistances were evaluated over their true perimeter areas. The open-ended, steel SD piles' first-time, tension loading curves are presented in Fig. 8 along with tests by Buckley *et al.* (2018a) on identical piles. Average  $\tau_{rzf}$  failure values varied from 30.2 to 142.3 kPa, with the  $w/D$  ratios at which the maximum load was obtained increasing from  $\approx 0.02$  to 0.07 as the piles aged.

*Inert stainless steel open pile.* The stainless steel SD18 pile developed the lowest tension  $\tau_{rzf}$ , which was only 20% greater than its (compressive) EoD  $\tau_{rzi}$ . If, after Vinck (2021), compression shaft capacities are treated as double those in tension, then the like-for-like set-up ratio  $\Lambda(t)$  is  $2[\tau_{rzf}(\text{tension})/\tau_{rzi}(\text{compression})] \approx 2.4$  after 125 days.

*Oxidisable steel open piles.* The oxidisable S355, L80/N80 and drill casing open SD piles developed far higher  $\Lambda(t)$  factors. Assuming again a compression/tension ratio = 2, piles SD12 and DP6-T1 showed, after 318 and 246 days, respectively, the highest  $\approx 154.1 \pm 15.5$  kPa resistances and maximum  $\Lambda(t) = 8.15$ . Interface shear tests against oxidisable X80 and S355 steels showed chalk  $\delta'_{ult}$  angles growing modestly from  $\approx 32^\circ$  to  $\approx 34.5^\circ$  after long-term ageing with access to air and water (Vinck, 2021). So other processes, which do not act around stainless steel piles, such as radial effective stresses building as corrosion products expand out radially into the very stiff chalk mass, are required to explain the oxidisable piles' long-term set-up above the water table.

Hammer size also affected the piles' EoD resistances and long-term capacities. Buckley *et al.*'s (2018a) piles, driven with a 4 ton Junttan SHK100-4 hammer that was  $\approx 2.9$  times heavier than that adopted for the ALPACA SD installations (see Table 5), gave particularly high long-term resistances and  $\Lambda$  values. Carroll *et al.* (2020) noted similar trends with piles driven in sand. Each hammer blow applies an extreme load cycle; it is plausible that less de-structuration occurs beneath pile tips and around shafts when larger hammers deliver significantly lower blow counts.

Figure 9 explores local shaft capacity trends by comparing the 318 days age tension  $\tau_{rzf}$  profile deduced SD12's FBG strain gauges with its dynamic (compression) EoD profile from Fig. 3(a). Set-up is evident over the whole shaft and most intensive over the mid-section. Also shown is a Chalk ICP-18 prediction evaluated employing the 'long-term' expressions given by Jardine *et al.* (2018) and Buckley *et al.* (2020a) with  $\delta'_{ult} = 32^\circ$ . While the latter offers a similar shape to the field data, integration indicates non-conservative overall calculated-to-measured capacity ratios,  $Q_c/Q_m \approx 1.74$  and  $\approx 1.14$  for SD12 and DP6-T1, respectively. As set out further below, these and other results identified a clear need to revise the Chalk ICP-18 procedures.

*Closed-ended steel and concrete piles.* Sampling and laboratory testing, undertaken after the pile experiments, identified the annular zone of chalk that had consolidated to far lower water contents after being reduced to putty by

**Table 7. Operational shear moduli derived from linear elastic analyses of initial loading stages of monotonic pile tests**

Pile	$D$ : m	$L_p$ : m	Initial pile stiffness: kN/mm	$G_{ope}$ : MPa	$G_{ope}/G_{max}$	Note*
SD12	0.139	5.35	584.7	313.0	0.22	
LD5	0.508	10.16	2080.5	451.9	0.31	
LD6	0.508	10.16	1906.9	381.4	0.26	
LD7	0.508	10.16	1982.5	409.7	0.28	
LD12	0.508	3.05	1798.8	393.7	0.27	
LD13	0.508	3.05	1864.6	412.9	0.28	
TP1	1.8	18	3252.0	222.2	0.15	
TP3	0.508	18	1212.3	279.9	0.19	
TP2†	1.22	7.3	3554.4	364.2	0.25	Compression
R1†	1.22	7.3	3883.5	422.3	0.29	Compression

\*Tests in tension unless otherwise noted.

†TP1 loaded in tension, reacting against piles TP2 and R1.

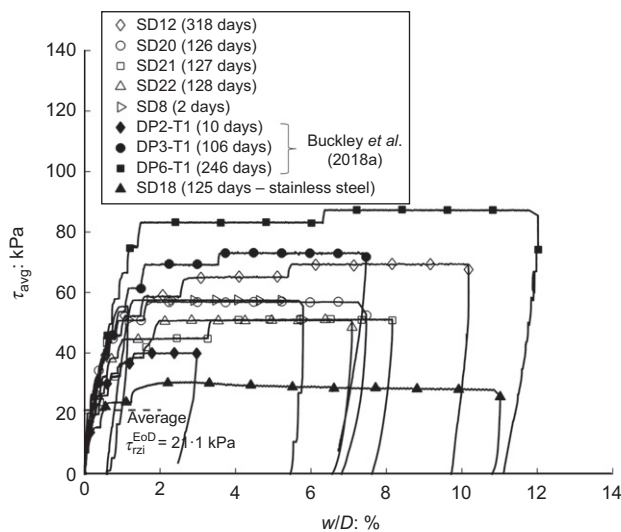


**Fig. 8. Trends for average shaft resistance ( $\tau_{avg}$ ) plotted against normalised pile head displacement ( $w/D$ ) for open-ended SD piles embedded fully above water table**

driving. The zone extended out to  $\approx D/2$  (or  $D^*/2$  for square piles) and to far smaller distances  $\approx t_w$  around open piles.

Figure 10 presents the long-term tension load–displacement plots for three closed-ended piles. The 73.4 kPa  $\tau_{zlf}$  achieved by the closed steel SD5 indicates an early-age  $\Lambda = 7.45$  after pore pressure and local stress equalisation (assuming again a compression/tension ratio = 2), far above the average short-term  $\Lambda = 2.7$  shown by the lower-displacement open piles. Long-term ageing added a further 53 kPa of tension shaft resistance to the twin SD7 pile over 329 days, giving a remarkable long-term ‘compression’  $\Lambda(t) = 14.4$ .

The solid and inert (factory) pre-cast reinforced concrete pile, whose driving permitted greater pore pressure dissipation during driving, also showed a relatively high (125 kPa) long-term tension resistance, reflecting the combined effects of its high driving resistance, post-EoD residual excess pore pressure dissipation and potentially in situ carbonate bonding; see Neugebauer (1975). However, assuming the compression shaft capacity was double that in tension (as with steel piles) indicates a lower long-term  $\Lambda(t) \approx 3$  than was developed by the more rapidly driven, and actively corroding, closed steel pile. The closed-end piles failed with  $0.03 < w/D < 0.07$  and their relatively high shaft capacities gave an average  $Q_c/Q_m \approx 1.0$  when compared to Chalk ICP-18 predictions.

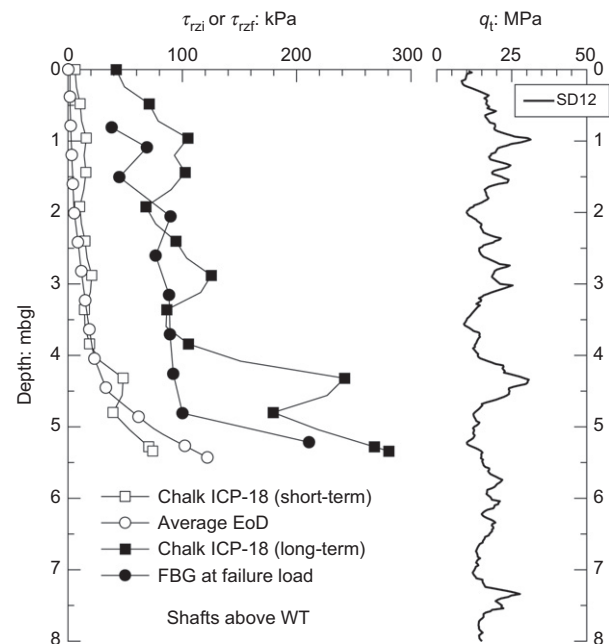


**Fig. 9. Comparison of shaft resistance profiles for SD12 determined from EoD PDA, short- and long-term Chalk ICP-18 predictions and fibre Bragg grating (FBG) measurements at peak failure load. CPT profile also shown**

The sheet pile tests also showed remarkable set-up. SD10's tension resistance rose well above its EoD compression capacity when, after 3 days, it could not be failed with the equipment deployed. Corrosion led to a 35% stiffer load–displacement curve after 317 days for the twin SD9 sheet pile and a remarkable average  $\tau_{zlf} > 205$  kPa applying after a displacement ratio  $w/D = 0.055$ .

**Short LD piles.** Figure 11 presents the short 508 mm OD X80 steel piles' curves after driving to 3.05 m penetrations. Their  $\tau_{zlf}$  profiles, deduced from FBG gauges, are given in Fig. 12, with EoD wave matches from Fig. 3(c) and long-term Chalk ICP-18 predictions. The piles failed with  $w/D < 0.035$  and average (tension)  $\tau_{zlf}$  around 3.9 times the compressive  $\tau_{zli}$  values, indicating long-term ‘compression’  $\Lambda(t)$  ratios  $\approx 7.9$  slightly below the SD piles' maxima and reflecting similar long-term processes above the water table, with set-up being greatest over the mid- and lower shaft sections. Long-term ICP-18 calculations capture the maximum observed local resistances (up to 270 kPa), but

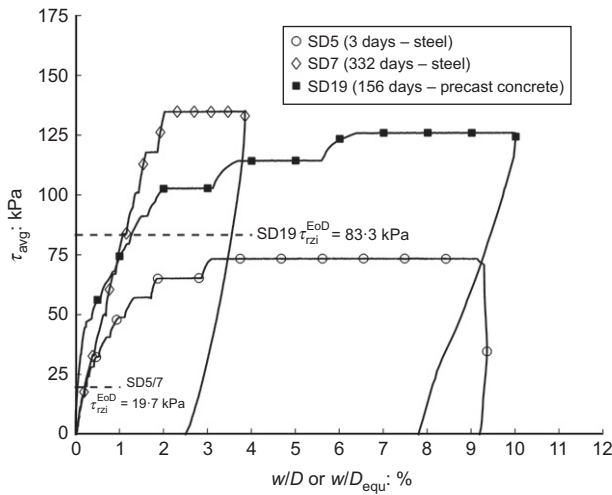


Fig. 10. Trends for  $\tau_{avg}$  plotted against  $w/D$  (or  $w/D_{equ}$ ) for closed-ended tubular steel and square concrete piles. ICP-18 predicts  $\tau_{avg} = 163.0$  and  $145.1$  kPa for SD7 and SD19

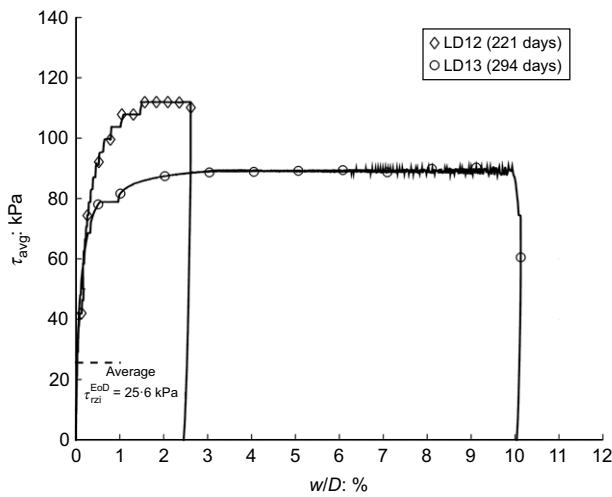


Fig. 11. Trends for  $\tau_{avg}$  plotted against  $w/D$  for LD12 and LD13 ( $D/t_w \approx 24.7$ ;  $L_p/D = 6$ ) embedded fully above water table. ICP-18 predicts  $\tau_{avg} = 162.0$  and  $155.2$  kPa for LD12 and LD13

again overestimate the overall tension capacities, giving  $Q_c/Q_m \approx 1.60$ .

#### Piles driven entirely below the water table

The ALPACA programme included five piles driven through holes pre-bored and cased to avoid contact with unsaturated chalk. As shown in Fig. 13(a), the slowly driven, closed-ended, solid concrete SD17 ( $L/D^* \approx 47$ ) developed higher long-term resistance below the water table than the equivalent concrete pile (SD19) above the water table. While tensile straining in SD17's 6.5 m of free shaft length led to larger pile head movements, this inert pile's development of a 'compression equivalent'  $\Lambda > 3.3$  was not affected by being submerged.

In contrast, the far higher  $L/D$  ( $\approx 90$ ) and consequent flexibility of the 139 mm OD steel tubes led to these piles 'whipping' during driving which, as noted by Lord *et al.* (2002), can halve capacity in low- to medium-density chalk. The piles' 6.5 m unrestrained free lengths allowed them to deflect easily during assembly and testing, potentially further damaging their axial capacity. Fig. 13(b) presents their

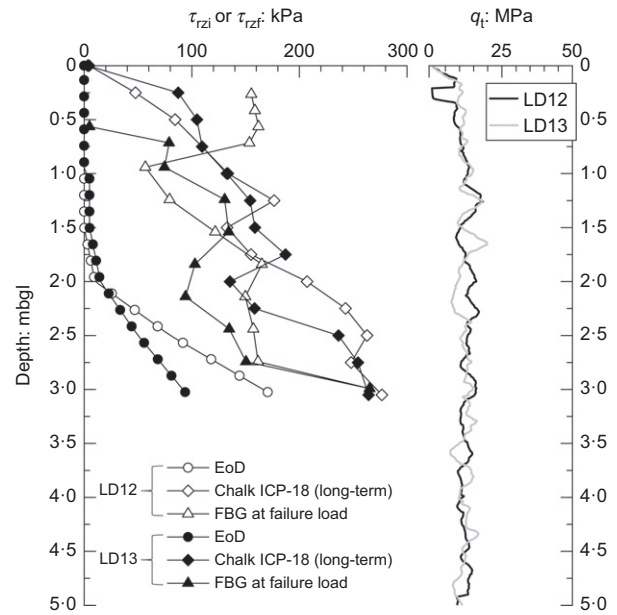


Fig. 12. Short- and long-term shaft resistance profiles for LD12 and LD13 from EoD, long-term Chalk ICP-18 predictions and FBG measurements at peak failure loads. CPT profile also shown

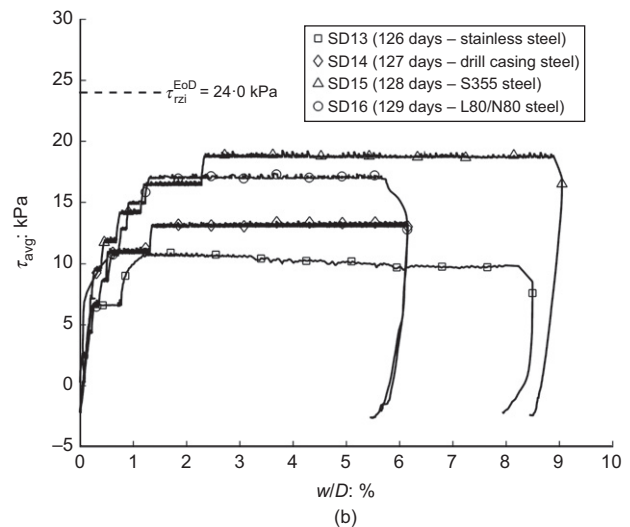
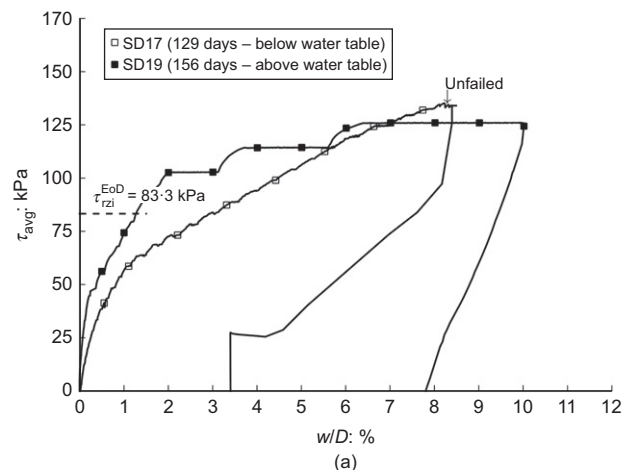


Fig. 13. Trends for  $\tau_{avg}$  plotted against  $w/D$  (or  $w/D_{equ}$ ) for (a) precast concrete piles and (b) cased SD13-SD16 steel piles embedded fully below water table. ICP-18 predicts  $\tau_{avg} = 249.0$  and  $145.1$  kPa, respectively, for SD17 and SD19, and on average  $116.3$  kPa for SD13-16

tension load–displacement curves after 126 to 129 days of ageing, all failing at average low  $\tau_{\text{zf}}$  (10.7 to 18.7 kPa) and  $w/D < 0.03$ . Stainless steel SD13 showed the lowest resistance. Assuming a compression-to-tension ratio of 2 indicates  $\Lambda = 0.9$ , well below the 2.4 applying (at a similar age) to the shorter and less flexible stainless steel SD18 driven above the water table. The oxidisable high  $L/D$  piles showed greater capacities below the water table, indicating that corrosion also contributed (albeit modestly and slowly) to their set-up. Highly flexible piles driven with long unsupported sections clearly develop abnormally low capacities.

#### Piles with shafts above and below the water table

**Long LD piles.** Tension tests on open 508 mm LD piles driven to 10.16 m ( $L_p/D = 20$ ) are presented in Fig. 14, all failing with  $w/D < 0.02$ . Average  $\tau_{\text{zf}}$  grew from 21.2 kPa (after 66 days) to 39.1 kPa at  $t > 200$  days, while the ‘equivalent compression’ long-term  $\Lambda(t)$  values grew from  $\approx 1.8$  to  $\approx 3.3$  over the same age interval. Fig. 5 collates their trends with those from other piles whose shaft capacities developed mostly below the water table. The compression test pile, LD7, illustrated in Fig. 15, indicated  $\Lambda = 3.45$  at 260 days, although the assessment depends on how loads are extrapolated over the lowest (0.65 m) shaft length. Fig. 15 also shows the average shear stresses evaluated for LD5, LD6 and LD7 down to the deepest strain gauge; the indicated tension  $\tau_{\text{zf}}$  values are lower than those shown in Fig. 14 because the final 0.65 m contributes so heavily to capacity.

Much of the compression pile’s greater resistance developed over its  $0.005 < w/D < 0.075$  range, where tangent stiffness slowly reduced towards zero at failure. This is interpreted as reflecting outward Poisson pile straining gradually raising shaft  $\sigma_r$  and hence  $\tau_{\text{zf}}$  stresses as growing shaft and base loads compress the shaft and expand it radially. The ratio of compression to tension shaft capacity from LD5 and LD6 is displayed in Fig. 16 together with Vinck’s (2021) assessment from similarly paired tests undertaken near Dieppe (France) and Hamburg (Germany) with comparable piles and chinks. An average ratio of at least 2 is indicated, which, as discussed later, was confirmed by long-term ALPACA-Plus tests.

The base capacity (1251.3 kN) mobilised at  $w/D = 0.075$  was found by projecting loads to the tip depth. It exceeds the driving and short-term re-drive tip loads detailed in Tables 1–4, indicating significant set-up and a resistance

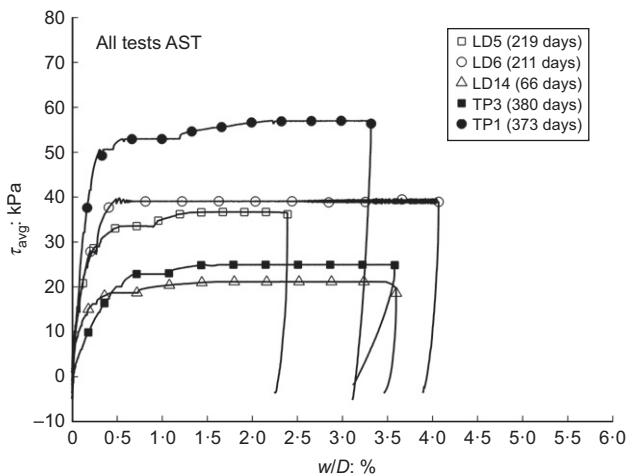


Fig. 14. Trends for tension  $\tau_{\text{avg}}$  plotted against  $w/D$  for the long LD piles and ALPACA-Plus piles. ICP-18 predicts  $\tau_{\text{avg}} = 141.5$ , 115.1, 99.5 and 144.5 kPa for LD5, LD6, TP3 and TP1, respectively

$q_b = 6.2$  MPa over the entire base area  $\approx 0.4q_t$ . Significant loads may have been transferred into the lowest section of the pile shaft through local internal shaft friction, as argued for sands by Jardine *et al.* (2005). Any internal shaft friction that develops above the lowest strain gauge level is effectively counted as combined with the external shaft resistance. Vinck (2021) provide further guidance based on long-term tests at other sites.

Local  $\tau_{\text{zf}}$  profiles are plotted in Fig. 17 for LD5, 6 and 7. Also shown are the typical EoD profile from Fig. 3(c) and long-term Chalk ICP-18 predictions. The compression test shows notably higher shaft resistance over its top half, where corrosion was most active, and the pile axial loads (and hence Poisson strains) were greatest. Nevertheless, the long-term Chalk ICP-18 predictions exceed the compression shaft capacity by 60% and those of the tension tests by a larger margin.

#### ALPACA-Plus piles driven to 18 m depth

The 18 m long TP1 and TP3 piles’ tension tests, conducted 373 and 380 days after driving, reached failure with  $w/D \approx 0.02$ , as shown in Fig. 14. Their set-up trends are identified in Fig. 5, while Fig. 18 presents their EoD and monotonic test  $\tau_{\text{zf}}$  profiles.

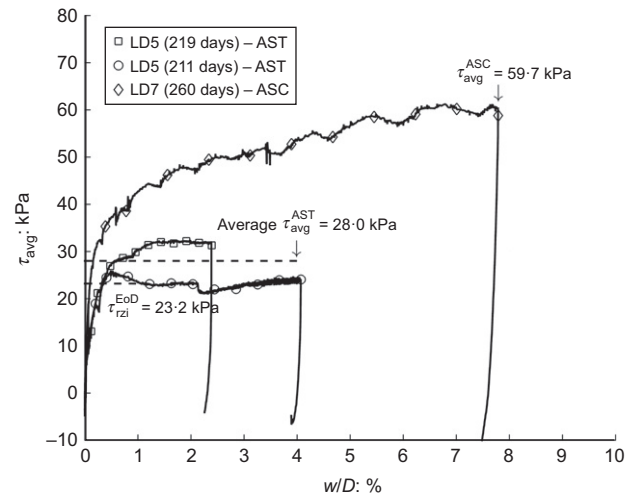


Fig. 15. Trends for  $\tau_{\text{avg}}$  plotted against  $w/D$  for long LD piles over the top 9.5 m section. ICP-18 predicts  $\tau_{\text{avg}} = 132.2$ , 104.8 and 106.3 kPa, respectively, for LD5, LD6 and LD7 over the same sections

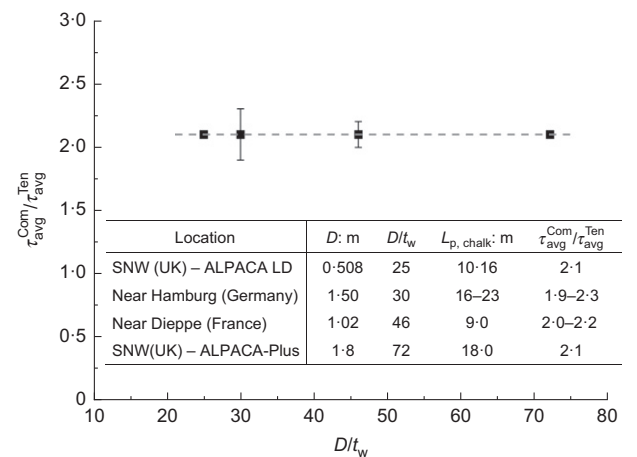


Fig. 16. Compression-to-tension shaft capacity ratios determined from tests at SNW and other cases collated by Vinck (2021)



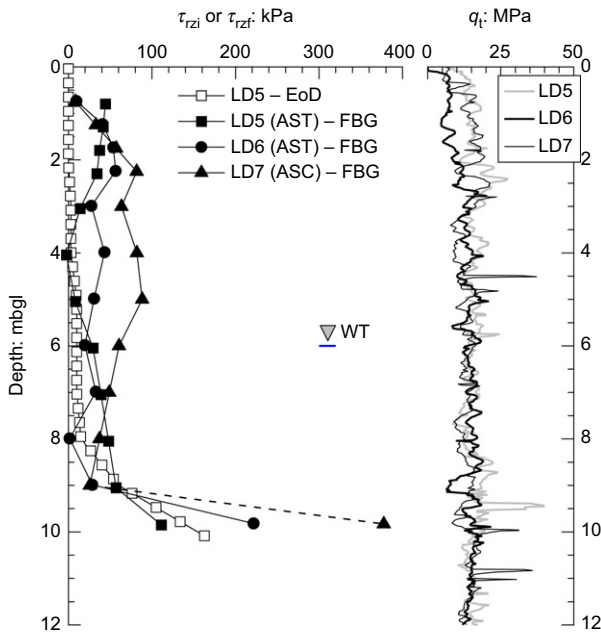


Fig. 17. Shaft resistance profiles for long LD piles (211–260 days aged) subjected to static tension (AST) and compression (ASC) axial loading. CPT profile also shown

Sharp reductions in local resistance with  $h/R$  led to the 1800 mm dia. ( $L_p/D = 10$ ) TP1 pile's average tension  $\tau_{rzi}$  (57.0 kPa) being more than double that (24.9 kPa) of the 508 mm dia. TP3, whose  $L_p/D = 35.4$ . Fig. 18 shows the local profiles that led to a 'compression equivalent'  $\Lambda(t) = 4.31$  for TP1, which exceeds the  $\approx 3.4$  reached by LD piles (with  $L_p/D = 20$ ), while TP3, the most slender pile, gave  $\Lambda(t) = 1.85$ . As shown in Fig. 5, set-up declines with  $L_p/D$ . Chalk ICP-18 calculations for the TP1 and TP3 tension tests give  $Q_c/Q_m$  as 2.6 and 4.0, respectively.

The 421 day re-strike on the 18 m long, 1220 mm OD, R2 pile indicated average  $\tau_{rzi} = 117.4$  kPa in compression, 2.1 times TP1's tension resistance (57.0 kPa), supporting the

trend of compression to tension capacity in Fig. 16. A still higher ratio may be inferred if allowance is made for R2's higher, and less advantageous,  $L_p/D$ .

#### Overall trends

The ALPACA and ALPACA-Plus axial tests identified ten clear trends.

- Open-ended and sheet steel piles develop notably lower driving resistances than closed steel and concrete piles.
- Piles driven at the same site show average long-term  $\tau_{rzi}$  values ranging from  $< 11$  kPa to  $> 200$  kPa.
- Closed-ended piles displace and de-structure a more extensive region of chalk than open piles. This feature may explain their far higher driving and long-term shaft resistances, as implied, for example, by cylindrical cavity expansion analyses of pile installation effects; see Randolph *et al.* (1979) or Carter *et al.* (1980).
- Highly flexible piles that 'whip' during driving develop anomalously low long-term shaft capacities.
- Short-term and long-term shaft resistances fall steeply with  $h/R^*$  or  $h/R$  in all cases.
- Marked set-up commences immediately after driving as pore pressures dissipate and total stresses evolve towards equilibrium values under the highly kinematically constrained conditions applying near the pile shafts.
- Further long-term set-up takes place above and below the water table at gradually slowing rates.
- Corrosion reactions lead to set-up being notably faster (i) around oxidisable steel piles driven above the water table and (ii) with saline rather than fresh groundwater.
- Compression shaft resistances appear to be at least twice as high as those available in tension.
- Chalk ICP-18 predicts driving SRD resistances with no overall bias and relatively low scatter, but over-predicts long-term capacity in most cases, indicating a need for careful re-calibration.

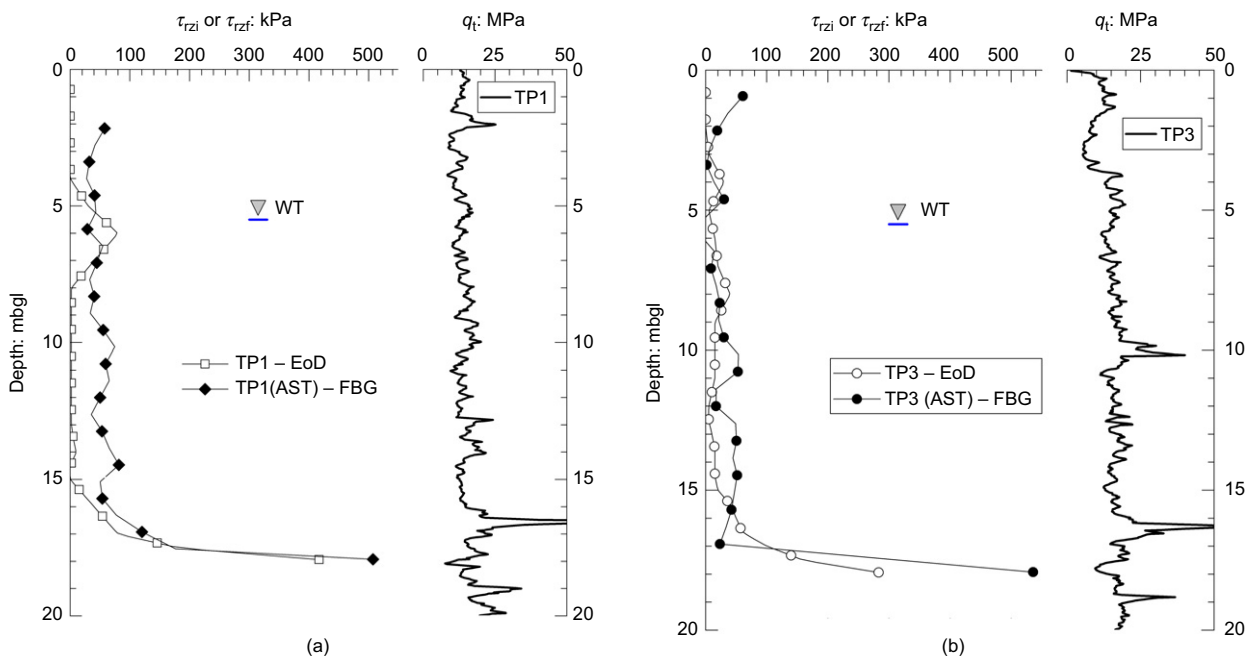


Fig. 18. Shaft resistance profiles for ALPACA-Plus piles (373–380 days aged) subjected to static tension (AST) axial loading: (a) TP1; (b) TP3. CPT profile also shown

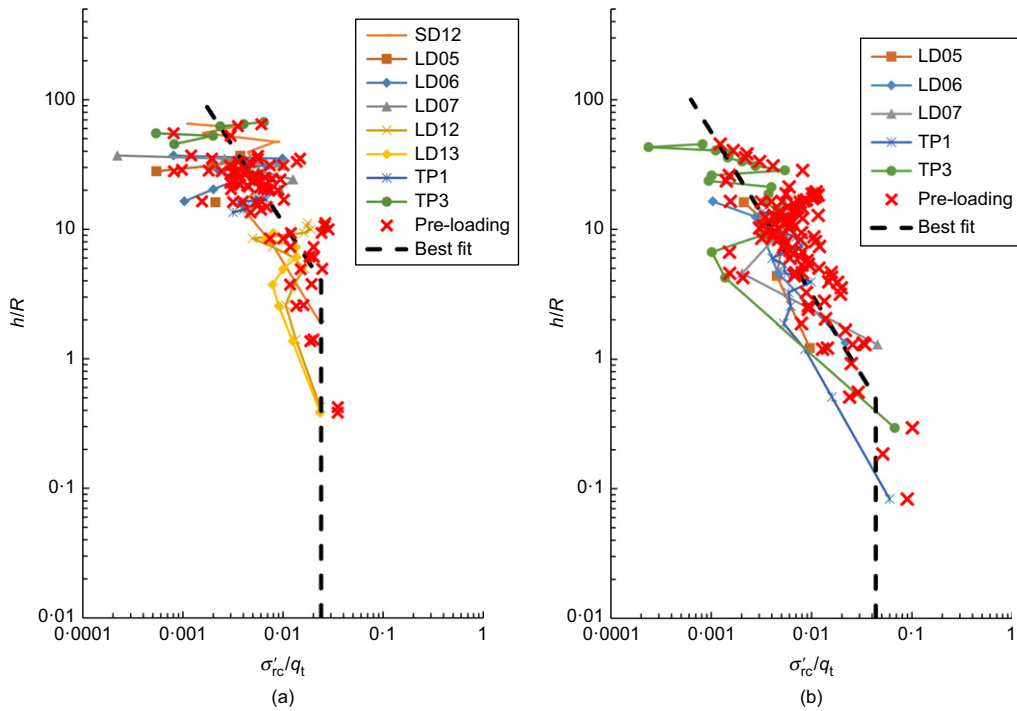


Fig. 19. Trends of  $h/R$  plotted against pre-loading  $\sigma'_{rc}/q_t$  for (a) above water table and (b) below water table

Table 8.  $Q_c/Q_m$  statistics for three axial capacity prediction methods, assessed against long-term monotonic measurements made in the ALPACA, ALPACA-Plus and earlier Innovate UK (Buckley *et al.*, 2018a) studies on 16 piles at SNW, excluding the stainless piles and the anomalous  $L/D = 90$  SD pile outcomes

Method	$Q_c/Q_m$ – whole shafts spanning water table depth			$Q_c/Q_m$ – above water table			$Q_c/Q_m$ – below water table		
	Mean	Standard deviation	CoV	Mean	Standard deviation	CoV	Mean	Standard deviation	CoV
CIRIA	0.33	0.16	0.49	0.42	0.29	0.69	0.37	0.16	0.43
ICP-18	2.06	0.91	0.44	1.97	0.95	0.48	2.96	0.87	0.29
New method	1.00	0.16	0.16	1.05	0.27	0.26	1.08	0.24	0.23

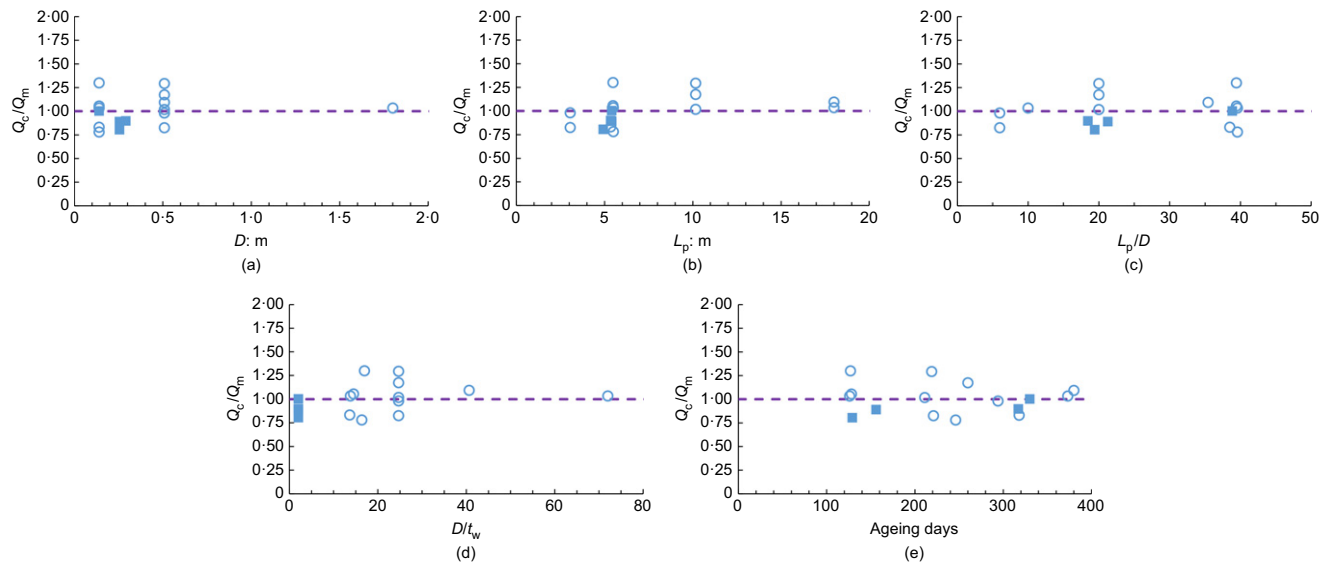


Fig. 20. Ratios between calculated and measured capacity ( $Q_c/Q_m$ ) plotted against (a)  $D$ , (b)  $L_p$ , (c)  $L_p/D$ , (d)  $D/t_w$  and (e) ageing days: open symbols represent open-ended piles; closed symbols signify closed-ended tubular, concrete and sheet piles. Covers all piles tested at ages  $\geq 120$  days except stainless steel cases and high  $L/D$  cased piles that showed whipping on driving



## RECALIBRATION OF LONG-TERM ICP CAPACITY METHOD

The ALPACA and ALPACA-Plus axial tests confirmed key general features of ICP-18's long-term shaft capacity formulation. However, they also proved the approach required significant recalibration to address the ten points itemised above. The first step was to expand the Coulomb criterion applied to characterise local shaft failure to recognise the impact of loading sense (compression or tension) on shaft capacity, as shown in equation (4).

$$\text{Local } \tau_{\text{rzt}} = f_L [\sigma'_{\text{rc}} + \Delta\sigma'_{\text{rd}}] \tan \delta' \quad (4)$$

For simplicity, loading factors  $f_L$  of 2/3 and 4/3 are taken for tension and compression that ensure a shaft capacity ratio of 2. These factors could be refined as further field or theoretical evidence emerges.

Updating is also required for the  $\Delta\sigma'_{\text{rd}}$  interface dilation term. As highlighted in Table 7, elastic analysis of the pile tests shows the operational shear modulus  $G_{\text{ope}}$  under pile loading is only 1/4 of that expected from seismic CPT testing. Adopting the finding by Lings & Dietz (2005) that shearing against fully rough interfaces induces a normal (dilative) displacement  $\Delta r$  in granular media comparable to their  $D_{50}$  grain size under the stress levels applying around pile shafts in chalk, leads to equation (5). Iterative analysis indicates that  $\Delta r$  may be taken as  $\approx 5 \mu\text{m}$  and  $\approx 3 \mu\text{m}$  above and below the water table, respectively.

$$\Delta\sigma'_{\text{rd}} = 4G_{\text{ope}}\Delta r/D \quad (5)$$

Applying Vinck's (2021)  $\delta' = 32^\circ$  and equations (4) and (5) to the  $\tau_{\text{rzt}}$ -depth profiles presented in Figs 9, 12, 17 and 18 leads to the pre-loading  $\sigma'_{\text{rc}}/q_t$  plotted against  $h/R$  trends in Figs 19(a) and 19(b) for conditions above and below the water table, respectively. The fitted power law relationships, given as equations (6) and (7), are subject to  $h/R$  minima, below which  $\sigma'_{\text{rc}}/q_t$  is constant. They capture markedly steeper  $\sigma'_{\text{rc}}/q_t$  decays with pile tip depth than Chalk ICP-18. They also employ  $h/R$  without any effective area term being required to avoid skewing with respect to  $D/t_w$  over the range considered of 15.4–80.8. Alternative correlations with  $h/R^*$  lead to marginally less satisfactory outcomes.

$$\begin{aligned} \text{Above water table : } \sigma'_{\text{rc}}/q_t &= f_{\text{tip}} \times 0.078 \\ &\times (h/R)^{-0.85} (h/R \geq 4.0) \end{aligned} \quad (6)$$

$$\begin{aligned} \text{Below water table : } \sigma'_{\text{rc}}/q_t &= f_{\text{tip}} \\ &\times 0.025 \times (h/R)^{-0.80} (h/R \geq 0.5) \end{aligned} \quad (7)$$

The pile-tip factor  $f_{\text{tip}}$  is 1 for the open piles considered and 3 for closed-ended piles. Intermediate factors may apply over the unexplored  $2 \leq D/t_w \leq 15.4$  range. Any 'internal' shaft resistance developed by open piles under compression loading is assumed to be built into these shaft and end bearing expressions; both sides of sheet piles are considered.

Integrating equations (4)–(7) over the pile shafts provides capacity predictions for 16 ALPACA, ALPACA-Plus and Innovate UK (Buckley *et al.*, 2018a) axial pile tests conducted at ages  $\geq 120$  days at the SNW site. Two deliberately 'non-standard' stainless steel piles (SD13 and 18) were excluded, so were the very high  $L_p/D$  open-ended steel SD piles driven through cased holes that had experienced whipping during installation. Table 8 summarises the mean  $Q/Q_m$  found with the recalibrated long-term approach for this dataset, showing unbiased means and relatively low CoVs for piles driven either entirely above or below the water table, as well as those that span both conditions. In

comparison, the CIRIA (Lord *et al.*, 2002) method is systematically over-conservative and Chalk ICP-18 non-conservative, largely because of the latter's assumption of equal tension and compression shaft capacities and less steep 'friction–fatigue' relationship. Set-up factors  $\Lambda$ , which vary strongly with  $L_p/D$ , may be assessed by dividing the calculated long-term capacities by the SRD values, which are generally well predicted by Chalk ICP-18.

The individual pile test points plotted in scatter diagrams in Fig. 20 confirm that the new method gives no significant bias with diameter  $D$ , length  $L_p$ ,  $L_p/D$ , wall thickness ratio,  $D/t_w$  or time over the  $\geq 120$  days age range.

Research remains active to assess how well the ALPACA-SNW approach predicts pile tests at other chalk sites, drawing on the case studies collated and reviewed by Vinck (2021) and other data. Further checking at other locations and in denser chalk strata is recommended.

## SUMMARY AND CONCLUSIONS

The ALPACA and ALPACA-Plus JIP programmes addressed the uncertain behaviour of piles driven in low-density to medium-density chalks through comprehensive dynamic, cyclic, monotonic, axial and lateral testing of piles covering a wide range of scales, materials, groundwater conditions, ages and loading modes, generating a unique high-quality experimental database against which design approaches may be assessed and developed. Buckley *et al.* (2023) reported the cyclic axial pile loading experiments and showed how their responses may be predicted from laboratory element tests and the 2022 final report of the ALPACA AWG to the JIP sponsors summarised the lateral loading study.

The main outcomes regarding monotonic axial loading are given below.

- Evidence of, and explanations for, a remarkably wide range of axial shaft resistances are provided, with: (i) pile end conditions and material; (ii)  $L_p/D$  ratio and flexibility; (iii) relative water table depth; (iv) age after driving; and (v) whether loading is compressive or tensile.
- Parallel information is revealed on load–displacement behaviour in tension and compression.
- It is demonstrated that driving resistances are generally well predicted by Chalk ICP-18, while long-term capacities are over-predicted by this approach. The CIRIA approach is shown to be generally over-conservative.
- A new ALPACA-SNW approach is proposed, which fits far more satisfactorily the widely ranging axial capacities measured at SNW on piles driven above or below the water table, when tested after at least 120 days after driving.
- Independent checking is underway to explore how well the approach performs in predicting research tests conducted at other sites in France, Germany and the UK; further high-quality testing at other sites is strongly recommended.

## ACKNOWLEDGEMENTS

The authors gratefully acknowledge support from Engineering and Physical Science Research Council (EPSRC) grant EP/P033091/1, Royal Society Newton Advanced Fellowship NA160438 and Supergen ORE Hub 2018 (EPSRC EP/S000747/1). B. Byrne is supported by the Royal Academy of Engineering under the Research Chairs and Senior Research Fellowships scheme, while K. Vinck was

supported by EPSRC grant EP/L016826/1, DEME and Imperial College. The provision of additional financial and technical support by the following project partners is also acknowledged gratefully: Atkins, Cathies, Equinor, Fugro, GCG, LEMS, Ørsted, Parkwind, RWE, Siemens-Gamesa, Scottish Power Renewables and Vattenfall. The authors also wish to acknowledge: Socotec UK Ltd as their main contractor for the field-testing programme; Marmota Engineering AG as the fibre optic strain gauge specialists; Cambridge in situ for the pressuremeter tests; and Lankelma UK and Fugro Geo-services for in situ testing and rotary boreholes.

## NOTATION

$c_h$	coefficient of horizontal consolidation
$D$	diameter of pile or penetrometer
$D^*$	equivalent pile diameter based on base area for cylindrical and square piles, and perimeter area for sheet piles
$D_{50}$	mean particle diameter
$D/t_w$	pile wall thickness ratio
$f_L$	axial compression or tension loading factor
$f_s$	cone penetration test (CPT) sleeve friction
$f_{tip}$	open- or closed-end tip condition factor
$G_{max}$	maximum shear modulus
$G_{ope}$	operational shear stiffness
$G_{vh}$	shear modulus in the vertical plane
$h$	distance from the pile tip
$k_s$	increment of creep displacement per log cycle of time
$L_p$	pile embedded length
$L_p/D$	pile length ratio
$Q_b$	pile base capacity
$Q_c/Q_m$	calculated to measured pile capacity
$q_t$	CPT cone resistance
$R$	pile radius
$R^*$	open-ended pile effective radius
$R_{CLA}$	centre-line-average surface roughness
$S_u$	undrained shear strength
$t_{100}$	full drainage elapsed time after end of driving
$t_w$	pile wall thickness
$V$	normalised velocity ( $= vD/c_h$ )
$v$	average pile penetration velocity
$W$	pile head displacement
$\Delta r$	radial dilation at pile interface
$\Delta\sigma'_{rd}$	change in radial effective stress due to interface dilation
$\delta', \delta'_{ult}$	ultimate interface friction angle
$\Lambda$	set-up factor
$\sigma'_r$	radial effective stress
$\sigma'_{rf}$	radial effective stress at failure
$\sigma'_z$	vertical effective stress
$\tau_{avg}$	average shaft resistance
$\tau_{rzi}$	shaft resistance at end of driving
$\tau_{zf}$	mobilised shaft resistance at failure
$\phi'_{cs}$	critical state shear resistance angle

## REFERENCES

- Baligh, M. M., Azzouz, A. S. & Chan, C. T. (1987). Disturbances due to ideal tube sampling. *J. Geotech. Engng* **113**, No. 7, 739–757.
- Barbosa, P. M., Geduhn, M., Jardine, R. J. & Schroeder, F. C. (2017). Large scale offshore static pile tests – practicality and benefits. In *8th international conference on offshore site investigation and geotechnics, smarter solutions for offshore developments*, vol. 1, pp. 644–651. London, UK: Society for Underwater Technology.
- Buckley, R. M. (2018). *The axial behaviour of displacement piles in chalk*. PhD thesis, Imperial College London, London, UK.
- Buckley, R. M., Jardine, R. J., Kontoe, S., Parker, D. & Schroeder, F. C. (2018a). Ageing and cyclic behaviour of axially loaded piles driven in chalk. *Géotechnique* **68**, No. 2, 146–161, <https://doi.org/10.1680/jgeot.17.P012>.
- Buckley, R. M., Jardine, R. J., Kontoe, S. & Lehane, B. M. (2018b). Effective stress regime around a jacked steel pile during installation ageing and load testing in chalk. *Can. Geotech. J.* **55**, No. 11, 1577–1591.
- Buckley, R. M., Jardine, R. J., Kontoe, S., Barbosa, P. & Schroeder, F. C. (2020a). Full-scale observations of dynamic and static axial responses of offshore piles driven in chalk and tills. *Géotechnique* **70**, No. 8, 657–681, <https://doi.org/10.1680/jgeot.19.TI.001>.
- Buckley, R. M., McAdam, R. A., Byrne, B. W., Doherty, J. P., Jardine, R. J., Kontoe, S. & Randolph, M. F. (2020b). Optimization of impact pile driving using optical Fiber Bragg-Grating measurements. *J. Geotech. Geoenviron. Engng* **146**, No. 9, 04020082.
- Buckley, R. M., Jardine, R. J., Kontoe, S., Liu, T., Byrne, B. W., McAdam, R. A., Schranz, F. & Vinck, K. (2023). Axial cyclic loading of piles in low to medium density chalk. *Géotechnique*, <https://doi.org/10.1680/jgeot.22.00044>.
- Burd, H. J., Beuckelaers, W. J. A. P., Byrne, B. W., Gavin, K. G., Houlsby, G. T., Igoe, D. J. P., Jardine, R. J., Martin, C. M., McAdam, R. A., Wood, A. M., Potts, D. M., Gretlund, J. S., Taborda, D. M. G. & Zdravković, L. (2020). New data analysis methods for instrumented medium-scale monopile field tests. *Géotechnique* **70**, No. 11, 961–969, <https://doi.org/10.1680/jgeot.18.PISA.002>.
- Carotenuto, P., Meyer, V., Strøm, P. J., Cabarkapa, Z., St. John, H. & Jardine, R. J. (2018). Installation and axial capacity of the Sheringham Shoal offshore wind farm monopiles – a case history. In *Engineering in chalk: proceedings of the chalk 2018 conference* (eds J. A. Lawrence, M. Preece, U. L. Lawrence and R. M. Buckley), pp. 117–122. London, UK: ICE Publishing.
- Carroll, R., Carotenuto, P., Dano, C., Salama, I., Silva, M., Rimoy, S., Gavin, K. & Jardine, R. J. (2020). Field experiments at three sites to investigate the effects of age on steel piles driven in sand. *Géotechnique* **70**, No. 6, 469–489, <https://doi.org/10.1680/jgeot.17.P185>.
- Carter, J. P., Randolph, M. F. & Wroth, C. P. (1980). Some aspects of the performance of open- and closed-ended piles. In *Numerical methods in offshore piling*, pp. 165–170. London, UK: Institution of Civil Engineers.
- Cathie, D., Jardine, R. J., Silvano, R., Kontoe, S. & Schroeder, F. (2022). Pile setup in sand – the ‘PAGE’ joint industry project. *11th international conference on stress wave theory and design and testing methods for deep foundations*, Rotterdam, the Netherlands, <https://doi.org/10.5281/zenodo.7148625>.
- Ciavaglia, F., Carey, J. & Diambra, A. (2017). Time-dependent uplift capacity of driven piles in low to medium density chalk. *Géotechnique Lett.* **7**, No. 1, 90–96, <https://doi.org/10.1680/jgele.16.00162>.
- De Nicola, A. & Randolph, M. F. (1993). Tensile and compressive shaft capacity of piles in sand. *J. Geotech. Engng* **119**, No. 12, 1952–1973.
- Doherty, P., Igoe, D., Murphy, G., Gavin, K., Preston, J., McAvo, C., Byrne, B. W., McAdams, R., Burd, H. J., Houlsby, G. T., Martins, M. C., Zdravkovic, L., Taborda, D. M. G., Potts, D. M., Jardine, R. J., Sideri, M., Schroeder, F. C., Muir Wood, A., Kallehave, D. & Skove Gretlund, J. (2015). Field validation of fibre Bragg grating sensors for measuring strain on driven steel piles. *Géotechnique Lett.* **5**, No. 2, 74–79, <https://doi.org/10.1680/geolett.14.00120>.
- Doughty, L. J., Buckley, R. M. & Jardine, R. J. (2018). Investigating the effect of ageing on the behaviour of chalk putty. *Engineering in chalk: proceedings of the chalk 2018 conference* (eds J. A. Lawrence, M. Preece, U. L. Lawrence and R. M. Buckley), pp. 695–701. London, UK: ICE Publishing.
- Finnie, I. M. S. & Randolph, M. F. (1994). Punch-through and liquefaction induced failure of shallow foundations on calcareous sediments. In *Proceedings of international conference on behaviour of offshore structures*, pp. 217–230. Oxford, UK: Pergamon.
- Hobbs, N. B. & Atkinson, M. S. (1993). Compression and tension tests on an open-ended tube pile in chalk. *Geotech. Engng* **26**, No. 3, 31–34.
- Jardine, R. J., Chow, F. C., Overy, R. F. & Standing, J. R. (2005). *ICP design methods for driven piles in sands and clays*. London, UK: Thomas Telford Ltd.
- Jardine, R. J., Buckley, R. M., Kontoe, S., Barbosa, P. & Schroeder, F. C. (2018). Behaviour of piles driven in chalk. *Engineering in chalk: proceedings of the chalk 2018 conference*

- (eds J. A. Lawrence, M. Preene, J. L. Lawrence and R. M. Buckley), pp. 33–51. London, UK: ICE Publishing.
- Jardine, R. J., Kontoe, S., Liu, T., Vinck, K., Byrne, B. W., McAdam, R. A., Schranz, F., Andolfsson, T. & Buckley, R. M. (2019). The ALPACA research project to improve design of piles driven in chalk. In *Proceedings of the XVII European conference on soil mechanics and geotechnical engineering, Reykjavik, Iceland, 1–6 of September 2019: geotechnical engineering, foundation of the future* (eds H. Sigursteinsson, S. Erlingsson and B. Bessason), <https://doi.org/10.32075/17ECSMGE-2019-0071>. Reykjavik, Iceland: Icelandic Geotechnical Society.
- Lings, M. L. & Dietz, M. S. (2005). The peak strength of sand–steel interfaces and the role of dilation. *Soils Found.* **45**, No. 6, 1–14.
- Liu, T., Ferreira, P., Vinck, K., Coop, M. R., Jardine, R. J. & Kontoe, S. (2023). The behaviour of a low-to-medium density chalk under a wide range of pressure conditions. *Soils Found.* **63**, No. 1, 101268, <https://doi.org/10.1016/j.sandf.2022.101268>.
- Lord, J. A., Clayton, C. R. I. & Mortimore, R. N. (2002). *Engineering in chalk, C574*. London, UK: CIRIA.
- Matthews, M. C., Clayton, C. R. I. & Own, Y. (2000). The use of field geophysical techniques to determine geotechnical stiffness parameters. *Proc. Instn Civil Engrs Geotech. Engng* **143**, No. 1, 31–42.
- Mortimore, R. N. (2013). The 11th Glossop Lecture: making sense of chalk: a total-rock approach to its engineering geology. *Q. J. Engng Geol. Hydrogeol.* **45**, No. 3, 252–334.
- Neugebauer, J. (1975). Some aspects of cementation in chalk. In *Pelagic sediments: on land and under the sea* (eds K. J. Hsu and H. C. Jenkins), ch. 7, pp. 149–176. Oxford, UK: Blackwell Scientific Publications.
- Randolph, M. F. (2008). *IMPACT – dynamic analysis of pile driving, manual*. Crawley, Australia: University of Western Australia.
- Randolph, M. F. & Wroth, C. P. (1978). Analysis of deformation of vertically loaded piles. *J. Geotech. Engng Div.* **104**, No. 12, 1465–1488.
- Randolph, M. F., Carter, J. P. & Wroth, C. P. (1979). Driven piles in clay – the effects of installation and subsequent consolidation. *Géotechnique* **29**, No. 4, 143–157, <https://doi.org/10.1680/geot.1979.29.4.361>.
- Su, R. K. L. & Zhang, Y. (2015). A double-cylinder model incorporating confinement effects for the analysis of corrosion-caused cover cracking in reinforced concrete structures. *Corros. Sci.* **99**, 205–218.
- Vinck, K. (2021). *Advanced geotechnical characterisation to support driven pile design at chalk sites*. PhD thesis, Department of Civil and Environmental Engineering, Imperial College London, London, UK.
- Vinck, K., Liu, T., Jardine, R. J., Kontoe, S., Ahmadi-Naghadeh, R., Buckley, R. M., Byrne, B. W., Lawrence, J., McAdam, R. A. & Schranz, F. (2022). Advanced in-situ and laboratory characterisation of the ALPACA chalk research site. *Géotechnique*, <https://doi.org/10.1680/jgeot.21.00197>.
- Vinck, K., Liu, T., Mawet, J., Kontoe, S. & Jardine, R. J. (2023). Field tests on large scale instrumented piles driven in chalk: results and interpretation. *Can. Geotech. J.*, <https://doi.org/10.1139/cgj-2022-0441>.
- Wang, Z. (2021). *Static and dynamic re-analysis of large-scale pile tests in chalk*. MSc dissertation, Department of Civil and Environmental Engineering, Imperial College London, London, UK.
- Wen, K., Kontoe, S., Jardine, R. J., Liu, T., Cathie, D., Silvano, R., Prearo, C., Wei, S., Schroeder, F. C. & Po, S. (2023). Assessment of time effects on capacities of large-scale piles driven in dense sands. *Can. Geotech. J.*, <https://doi.org/10.1139/cgj-2022-0060>.